Title

A Critical Appraisal of the “Day” Diagram

Journal

Journal of Geophysical Research: Solid Earth, 123(4)

ISSN

2169-9313

Authors

Roberts, Andrew P
Tauxe, Lisa
Heslop, David
et al.

Publication Date

2018-04-01

DOI

10.1002/2017jb015247

Peer reviewed

Journal of Geophysical Research: Solid Earth

RESEARCH ARTICLE
10.1002/2017JB015247

Special Section:
Magnetism in the Geosciences - Advances and Perspectives

A Critical Appraisal of the "Day" Diagram

Andrew P. Roberts[1], Lisa Tauxe[2], David Heslop[1], Xiang Zhao[1], and Zhaoxia Jiang[3]

[1]Research School of Earth Sciences, Australian National University, Canberra, ACT, Australia, [2]Scripps Institution of Oceanography, University of California San Diego, La Jolla, CA, USA, [3]Ocean University of China, Qingdao, China

Abstract The "Day" diagram (Day et al., 1977, https://doi.org/10.1016/0031-9201(77)90108-X) is used widely to make inferences about the domain state of magnetic mineral assemblages. Based on theoretical and empirical arguments, the Day diagram is demarcated into stable "single domain" (SD), "pseudo single domain" ("PSD"), and "multidomain" (MD) zones. It is straightforward to make the necessary measurements for a sample and to plot results within the "domain state" framework based on the boundaries defined by Day et al. (1977, https://doi.org/10.1016/0031-9201(77)90108-X). We discuss 10 issues that limit Day diagram interpretation, including (1) magnetic mineralogy, (2) the associated magnetocrystalline anisotropy type, (3) mineral stoichiometry, (4) stress state, (5) surface oxidation, (6) magnetostatic interactions, (7) particle shape, (8) thermal relaxation, (9) magnetic particle mixtures, and (10) definitional/measurement issues. In most studies, these variables are unknowns and cannot be controlled for, so that hysteresis parameters for single bulk samples are nonunique and any data point in a Day diagram could result from infinite combinations of relevant variables. From this critical appraisal, we argue that the Day diagram is fundamentally ambiguous for domain state diagnosis. Widespread use of the Day diagram has also contributed significantly to prevalent but questionable views, including underrecognition of the importance of stable SD particles in the geological record and reinforcement of the unhelpful PSD concept and of its geological importance. Adoption of approaches that enable correct domain state diagnosis should be an urgent priority for component-specific understanding of magnetic mineral assemblages and for quantitative rock magnetic interpretation.

Key Points:
- The Day diagram is a rock magnetic classic and has been used widely for domain state diagnosis
- We document details of 10 ambiguities associated with Day diagram interpretation, which undermine most uses of this favorite tool
- Domain state diagnosis requires use of tools for identifying individual magnetic components that is not possible with the Day diagram

Correspondence to:
A. P. Roberts,
andrew.roberts@anu.edu.au

Citation:
Roberts, A. P., Tauxe, L., Heslop, D., Zhao, X., & Jiang, Z. (2018). A critical appraisal of the "Day" diagram. *Journal of Geophysical Research: Solid Earth*, *123*, 2618–2644. https://doi.org/10.1002/2017JB015247

Received 16 NOV 2017
Accepted 26 MAR 2018
Accepted article online 30 MAR 2018
Published online 22 APR 2018

1. Introduction

The paper by Day et al. (1977) is a landmark publication in rock magnetism. Through measurement of a simple set of magnetic hysteresis parameters, Day et al. (1977) proposed a plot now known as the "Day diagram" that is used extensively to make inferences about the magnetic domain state of magnetic mineral assemblages. The parameters used to construct the Day diagram had previous use in rock magnetism (e.g., Néel, 1955; Wasilewski, 1973); Day et al. (1977) presented them graphically to produce what we refer to as the Day diagram. The coordinates of a Day diagram are the ratios of the saturation remanent magnetization to saturation magnetization (M_{rs}/M_s) and the coercivity of remanence to coercivity (B_{cr}/B_c), as determined from a major hysteresis loop (Figure 1a) and a backfield demagnetization curve (Figure 1b). M_s is a material constant for a magnetic mineral, whereas M_{rs} provides a measure of the maximum remanence value a magnetic particle can carry. For populations of ideal stable single domain (SD) particles, M_{rs} has relatively high values with respect to an applied field direction, whereas M_{rs} is low for multidomain (MD) particles because significant internal cancelation of magnetic moments occurs due to development of domain structures. Thus, M_{rs}/M_s is sensitive to magnetic domain state variations (e.g., Dunlop, 1986; Dunlop & Argyle, 1997; Dunlop & Özdemir, 1997; Hunt et al., 1995; Néel, 1955) (Figure 2a). As discussed below, M_{rs} is also sensitive to other factors such as the magnetic anisotropy type, including magnetocrystalline and shape anisotropy, and thermal fluctuations.

The domain state dependence of magnetic properties is not a result of any intrinsic particle size control. Rather, the magnetic domain state depends strongly on M_s so that when particle volume increases, the demagnetization energy increases proportionally to M^2, and a lower energy state is achieved by subdividing the internal magnetization structure of a particle into domains, which lowers M_{rs}. Both B_c and B_{cr} are also sensitive to domain state variations when particles are larger (or smaller) than the stable SD threshold size (Figures 2b and 2c) (e.g., Dunlop & Özdemir, 1997; Heider et al., 1996; Hunt et al., 1995; Maher, 1988; Nagata, 1961). Thus, in plots of M_{rs}/M_s versus B_{cr}/B_c (Figure 1c), data trends are interpreted in terms of magnetic domain state variations (Day et al., 1977). With increased availability of instruments that can measure hysteresis loops and backfield demagnetization curves rapidly (e.g., Flanders, 1991; Foner, 1959), the Day diagram has become a routine part of paleomagnetic, rock magnetic, and environmental magnetic studies over

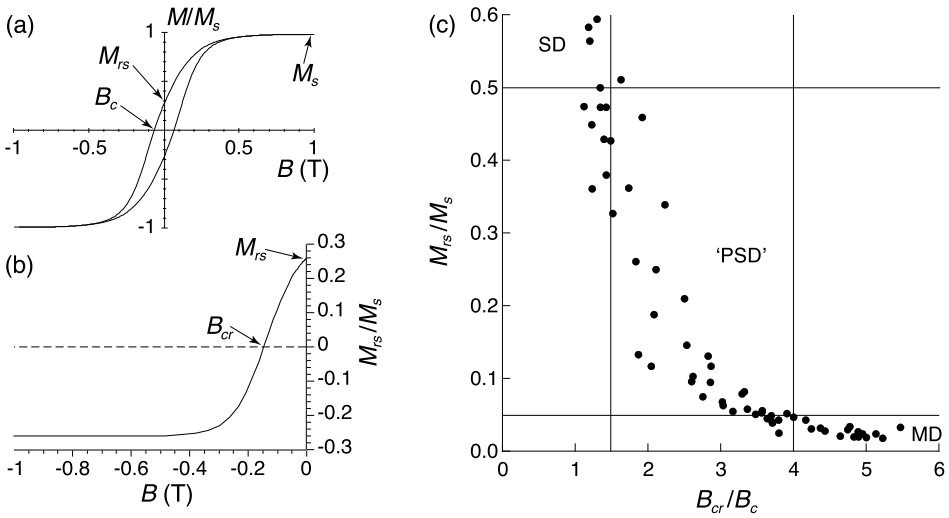

Figure 1. Definitions of hysteresis parameters and the Day diagram. (a) A major hysteresis loop with magnetization, M, normalized to the saturation magnetization, M_s. Definitions are shown graphically for the saturation remanent magnetization (M_{rs}) and coercivity (B_c). (b) Backfield demagnetization curve in which the remanent magnetization (M_r) is measured from saturation (M_{rs}), where it is demagnetized to zero at the coercivity of remanence (B_{cr}), and continues to negative saturation at $-M_{rs}$. (c) The original "Day" diagram reproduced from Day et al. (1977), with coordinates of M_{rs}/M_s and B_{cr}/B_c.

the last 25 years and is generally interpreted not just in terms of magnetic domain state but also in terms of magnetic granulometry. A key aspect of reliable hysteresis parameter determination is that saturating fields must be applied at identical peak fields for hysteresis loops and backfield demagnetization curves (Figure 1), and high-field slope correction of hysteresis loops must be done appropriately, as discussed in detail in section 2.10.2 of this paper.

Importantly, Day et al. (1977) pointed out that geological samples contain magnetic minerals with particle size distributions and that it is important to establish the effects of mixing of coarse and fine magnetic particles. They reported that for samples with variable concentrations of coexisting hard and soft magnetic fractions, hysteresis parameters can be influenced differentially, so that the effects of mixtures cannot be ignored in studies of the domain state dependence of hysteresis properties. Likewise, they pointed to the importance of minimizing magnetostatic interactions when analyzing synthetic magnetic particle assemblages and to understanding mineral stoichiometry when interpreting results in terms of magnetic domain state. Thus, key limitations of the Day diagram were known from the outset.

In addition to issues indicated by Day et al. (1977), several other factors complicate interpretation of the Day diagram. We argue in this paper that the extent of these deficiencies is likely to be so significant as to invalidate use of the Day diagram for domain state diagnosis without detailed additional information concerning mineralogy, the magnetic anisotropy type of constituent magnetic minerals, mineral stoichiometry, state of internal stress, surface oxidation, magnetostatic interactions, magnetic particle shape, and the number (and magnetic properties) of magnetic mineral components mixed within a sample. In this paper, we document evidence in relation to these factors of relevance to Day diagram interpretation and urge users to consider them when interpreting the Day diagram to assess whether associated uncertainties are sufficiently well constrained to allow the intended use. Additionally, as is already the case in the discussion so far, consideration of the Day diagram usually mixes concepts associated with particle size and domain state variations, where this might not be valid. For example, two particles with identical size but different stoichiometry could have different domain states. This ambiguity is fundamental to the Day diagram and is in addition to the issues mentioned above. Such ambiguities should be borne in mind when considering the issues discussed below.

2. Factors That Affect Data Distributions in a Day Diagram

2.1. Magnetic Mineralogy

A key aspect of the Day diagram that is often ignored is that it was defined for one of only two monomineralic magnetic particle systems (magnetite or titanomagnetite). Magnetic domain state transitions occur at

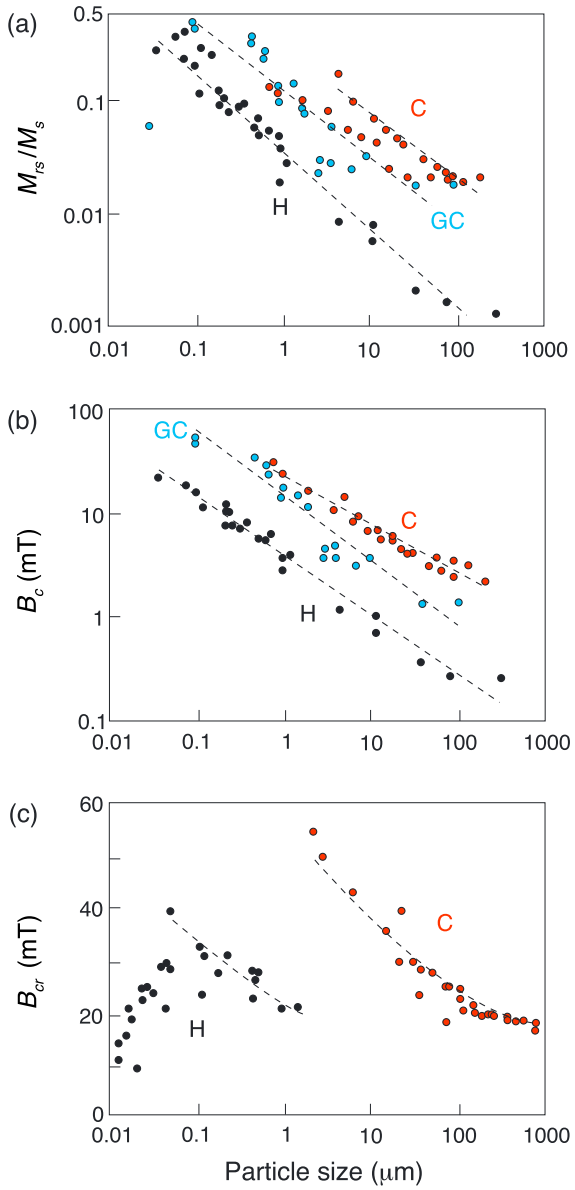

Figure 2. Illustration of the particle size dependence of hysteresis parameters for magnetite produced by different methods. Variations are shown for (a) M_{rs}/M_s, (b) B_c, and (c) B_{cr}. Red circles denote particles that were crushed (C) from larger magnetite grains and sieved to the specified size, blue circles denote magnetite produced by the glass ceramic (GC) method, and black circles denote magnetite grown from hydrothermal (H) solution. Data were compiled by Tauxe et al. (2010) from Hunt et al. (1995).

different particle sizes for different magnetic minerals. The principal controls on domain state threshold size are M_s and particle shape (e.g., Butler & Banerjee, 1975; Evans & McElhinny, 1969; Fabian et al., 1996; Muxworthy & Williams, 2009). The particle sizes at which the superparamagnetic (SP) to stable SD, stable SD to pseudo single domain ("PSD") (or flower then vortex states; Schabes & Bertram, 1988), and PSD to MD transitions occur vary considerably from mineral to mineral. For example, at room temperature the size range over which the stable SD state occurs in equant noninteracting particles varies from ~28 to ~75 nm in stoichiometric magnetite (Muxworthy & Williams, 2009), from ~46 to ~107 nm in greigite (Muxworthy et al., 2013), from 28 nm to 15 μm (Banerjee, 1971) or even 100 μm (Kletetschka & Wasilewski, 2002) in hematite, up to 1.5–3 μm in monoclinic pyrrhotite (Clark, 1984; Dekkers, 1988; Soffel, 1977), and up to 0.5–0.7 μm in titanomagnetite ($Fe_{3-x}Ti_xO4$) for x = 0.632–0.72 (Soffel & Appel, 1982), whereas in iron the SD state is not stable in equant particles at room temperature so that there is a direct transition from the SP to the single vortex state (Butler & Banerjee, 1975; Muxworthy & Williams, 2015). As a result, domain state variations for two co-occurring magnetic minerals within a single sample will be associated with different particle size ranges for each mineral. Comparing data for more than a single magnetic mineral in a Day diagram, therefore, comes with significant complications. This is illustrated further below.

2.2. Magnetocrystalline Anisotropy Type

A further parameter that depends on mineralogy is the type of magnetic anisotropy that controls the magnetization of the mineral. The maximum possible M_{rs} value depends on the number and orientation of magnetic easy axes (i.e., anisotropy) with respect to the applied field direction as well as on particle size. In rock magnetism, it is generally assumed that there are so many magnetic particles in a sample that their easy axes are distributed randomly with respect to the applied field direction. It is necessary to average the response of such randomly oriented easy axes with respect to the applied field. For example, if the magnetic easy axes of a population of uniaxial SD particles are all parallel to the applied field, the net saturation remanence will equal the saturation magnetization; if the easy axes are always perpendicular to the applied field, the net saturation remanence will be zero (Stoner & Wohlfarth, 1948). The two opposite directions along an easy axis in uniaxial particles are equivalent, so the magnetization can be aligned in either direction. Thus, for randomly oriented SD particles with uniaxial anisotropy over a hemisphere in a three-dimensional system, $M_{rs} = 0.5M_s$ (Stoner & Wohlfarth, 1948). This provides the theoretical basis for designating the SD/PSD threshold at $M_{rs}/M_s = 0.5$ (Day et al., 1977). In stable SD particles with cubic anisotropy and first anisotropy constant $K_1 > 0$, the easy direction is aligned along the <100> crystallographic axis and the magnetization will lie along one of the three <100> directions. Averaging for a random distribution of easy axes within a sample gives $M_{rs} = 0.831M_s$ for cubic crystals (Chikazumi, 1997; Joffe & Heuberger, 1974). For $K_1 < 0$ and an easy direction aligned along <111> in cubic crystals, $M_{rs} = 0.866M_s$ (Chikazumi, 1997; Joffe & Heuberger, 1974). Hematite has its magnetization confined within its basal plane with triaxial anisotropy; for randomly oriented hematite particles, $M_{rs}/M_s = 0.75$ (Dunlop, 1971). Thus, the maximum possible M_{rs}/M_s value depends on the type of anisotropy, where, for example, magnetite with elongation >~1.3 has a shape-dominated uniaxial anisotropy, while greigite has cubic anisotropy (Roberts et al., 2011), and hematite and monoclinic pyrrhotite have triaxial anisotropy within their basal planes (e.g., Martín-Hernández et al.,

2008; Özdemir & Dunlop, 2014). Magnetism in titanomagnetite is controlled by internal stress, which has usually been considered to be uniaxial. Gee and Kent (1995) argued from hysteresis data with $M_{rs}/M_s > 0.5$ that titanomagnetite has cubic anisotropy, which was later revised to multiaxial rather than strict cubic anisotropy because of the large observed coercivities that are not consistent with cubic anisotropy and that are hidden in the Day diagram by normalization of B_{cr} by B_c (Tauxe et al., 2002). The magnetic anisotropy type is important, therefore, because it controls the allowable range of values in the parameter space represented by a Day diagram. The assumption of uniaxial anisotropy can be invalid because multiaxial anisotropy may be more common in nature than has generally been assumed (e.g., Mitra et al., 2011).

For most magnetic mineral assemblages dominated by (titano)magnetite, data fall within the PSD region regardless of whether SP, SD, flower, vortex, or MD particles are present (Figure 3) because contributions from all particles in a sample average to fall within this intermediate region of the Day diagram. This produces a strong contrast when magnetite co-occurs with minerals such as monoclinic pyrrhotite (Figure 4), which have different magnetic anisotropy types and generally contrasting M_{rs}/M_s values (Rochette et al., 1990). In this situation, it is principally the anisotropy difference that gives rise to the marked contrast in data distributions in a Day diagram rather than intrinsic particle size differences. Magnetic particles at the "fine" end of the Day diagram could even be coarser than the magnetite that lies in the PSD region. This is evident from first-order reversal curve (FORC) diagrams (Pike et al., 1999; Roberts et al., 2000), which enable clearer diagnosis of domain state for both magnetic components illustrated in Figure 4 than the accompanying Day diagram. In Figure 4, the magnetite end-member has M_{rs}/M_s = 0.2–0.3, yet a significant SD particle assemblage is indicated clearly by the closed FORC contours for these samples. The reason that data for these samples plot at M_{rs}/M_s = 0.2–0.3 is because part of the magnetic mineral assemblage contains particles with lower M_{rs}/M_s values. These examples demonstrate how overreliance on a Day diagram can bias against recognition of SD particles. As discussed above, SD magnetite has finer sizes than co-occurring SD pyrrhotite, so the Day diagram (Figure 4) gives misleading absolute granulometric information and provides more information about the difference in anisotropy type in the co-occurring magnetic minerals.

A further example of the effect of anisotropy type on interpretation of hysteresis data involves mid-ocean ridge basalts (MORBs). M_{rs}/M_s values >0.5 and up to 0.67 have been reported in MORBs (Day et al., 1978; Gee & Kent, 1995), which led Gee and Kent (1995) to suggest that cubic anisotropy must be important in titanomagnetite. This interpretation was revised to refer to "multiaxial" anisotropy instead of cubic anisotropy because more complicated particle shapes are required to explain the observed high coercivities that are not expected for cubic anisotropy (Tauxe et al., 2002). Fabian (2006) questioned the origin of the reported M_{rs}/M_s values >0.5, but the interpretation of multiaxial anisotropy was later supported by additional evidence (Lanci, 2010; Mitra et al., 2011; see the comment and reply by Fabian, 2012; Mitra et al., 2012). Titanomagnetite is the main magnetic mineral in MORB, which covers 65% of Earth's surface (Moores & Twiss, 1995) and occurs commonly in other igneous and derivative sedimentary rocks. Thus, the potential for complications in Day diagrams due to contrasting magnetic anisotropy types in different constituent magnetic minerals is significant, particularly when considering mixed magnetic particle assemblages (see section 2.9).

2.3. Mineral Stoichiometry

Day et al. (1977) presented hysteresis data for magnetite and titanomagnetite assemblages with variable particle sizes and Ti contents (i.e., the x value in $Fe_{3-x}Ti_xO_4$). In their original Day diagram, all data were grouped regardless of particle size and x value, as reproduced in our Figure 1c. The representation in Figure 1c masks a key dependence of hysteresis parameters on titanomagnetite stoichiometry, which becomes obvious when plotting the tabulated data of Day et al. (1977) for four sets of samples with particle sizes that vary from 0.8 μm to >100 μm, with compositions that vary from x = 0 to 0.6 (Figure 5a). With varying x, samples with a nominal "0.8 μm" particle size have M_{rs}/M_s values that range from 0.47 to 0.13 (i.e., from almost the SD region to the MD region for identical particle sizes). Likewise, for coarse samples with nominal sizes >100 μm, M_{rs}/M_s is almost constant, but B_{cr}/B_c varies from 3.80 to 5.47 with the highest of these values for a sample that is nominally ~30 μm smaller than for the lowest value. Ti content in titanomagnetite is, therefore, an important determinant for interpretation of the Day diagram. Day et al. (1977) stated that this compositional dependence of hysteresis parameters reduces the usefulness of the eponymous Day diagram if the

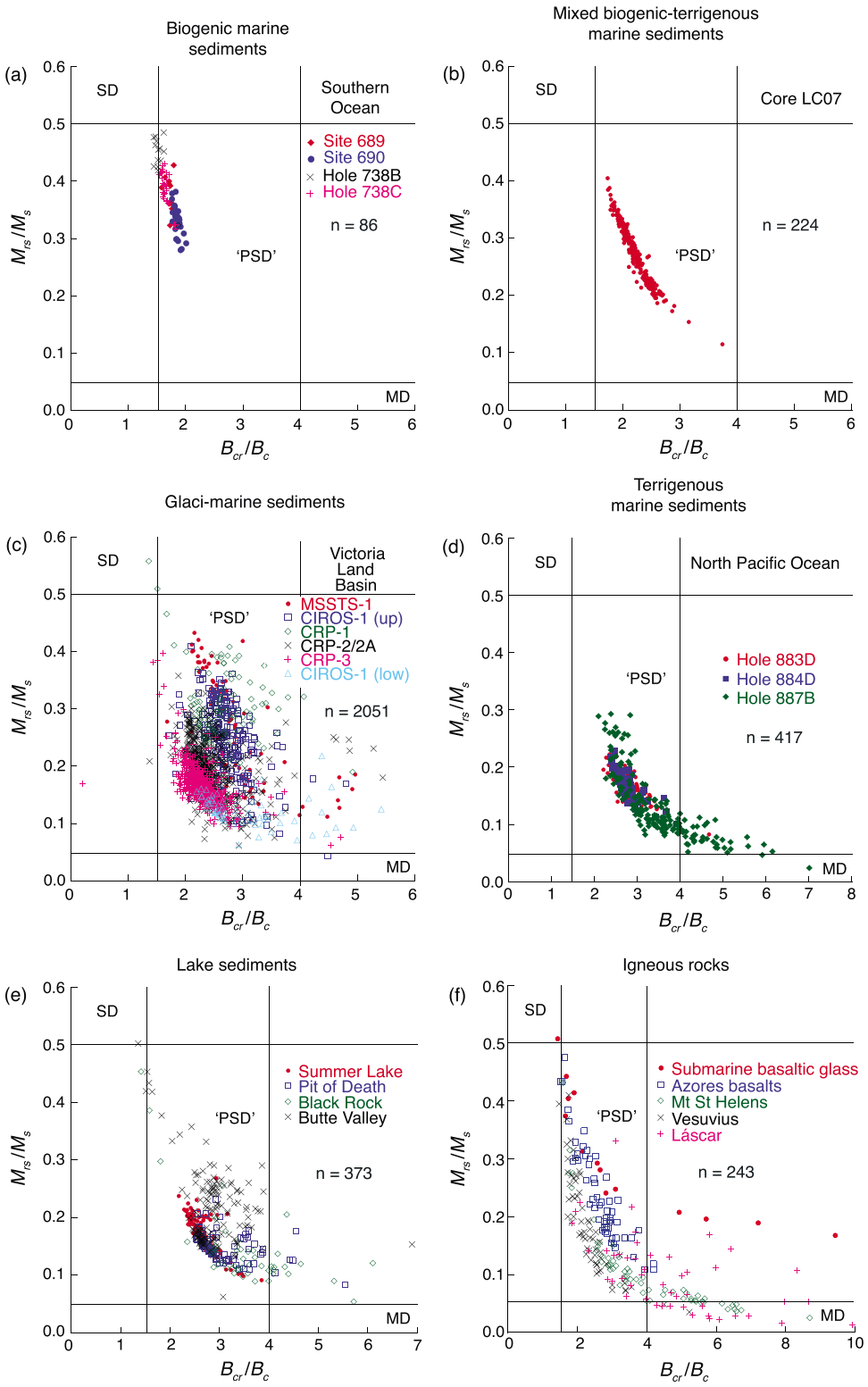

Figure 3. Illustration of Day diagrams for >3,300 sediment and igneous rock samples with magnetic properties dominated by Fe-Ti oxides. (a) Biogenic-dominated marine sediments from the Southern Ocean (summarized by Roberts et al., 2012), (b) mixed biogenic-terrigenous marine sediments from the Mediterranean Sea (Dinarès-Turell et al., 2003), (c) glaci-marine sediment from Victoria Land Basin, Ross Sea, Antarctica (summarized by Roberts, Sagnotti, et al., 2013), (d) terrigenous marine sediments from the North Pacific Ocean (Roberts et al., 1995), and (e) various lake sediments from the Great Basin, western USA (summarized by Roberts et al., 2012). (f) Hysteresis results for igneous rocks, including submarine basaltic glass (Tauxe et al., 1996) and basalts from the Azores (Di Chiara et al., 2014) and from Mt St. Helens, USA, Mt Vesuvius, Italy, and Volcan Láscar, Chile (Paterson et al., 2010).

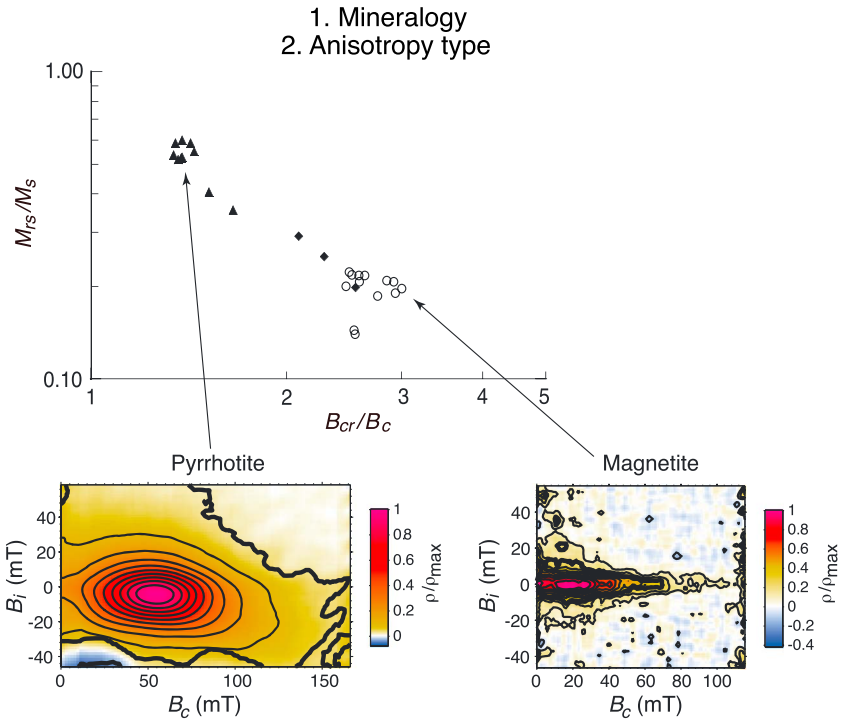

Figure 4. Illustration of the effect of mixing of minerals with different anisotropy types in Day diagrams. Mixture of strongly interacting SD pyrrhotite (multiaxial anisotropy) and noninteracting SP, SD, and coarser magnetite (uniaxial anisotropy) plotted on a Day diagram for Miocene mudstones from Sakhalin, Russia. Solid triangles: pyrrhotite-bearing samples; open circles: magnetite-bearing samples; and solid diamonds: mixed pyrrhotite- and magnetite-bearing samples. FORC diagrams provide information about the underlying domain state and interaction field distributions in the respective samples. Reproduced from Roberts et al. (2014) with results from Weaver et al. (2002). The smoothing factor (Roberts et al., 2000) is 5 for both FORC diagrams.

magnetic mineral composition is unknown. The composition of titanomagnetite particles in natural samples is rarely reported alongside published Day diagrams, and the caveat of Day et al. (1977) is rarely noted. Thus, the role of (titano) magnetite stoichiometry is a significant unknown in typical applications of Day diagrams.

2.4. Stress State

Magnetite is the most commonly occurring and most extensively studied terrestrial rock-forming magnetic mineral, and various compilations have been published of its magnetic hysteresis properties (e.g., Dunlop, 1986; Dunlop & Argyle, 1997; Dunlop & Özdemir, 1997; Heider et al., 1996; Hunt et al., 1995; Maher, 1988). In addition to a particle size dependence of hysteresis parameters, there is a profound dependence on the mode by which magnetite particles are produced (Figure 2). Three main magnetite sources are used in such studies: natural crystals that have been crushed (C) and sieved into specified grain size ranges, crystals that were grown with a glass ceramic (GC) technique, and crystals grown from hydrothermal (H) solution. Crushed particles generally have higher coercivities and remanence ratios than grown crystals (Figure 2), presumably because they contain larger numbers of lattice dislocations that stabilize domain walls. The high values observed for crushed particles largely disappear after high temperature annealing, which allows dislocations to "relax" away (Dunlop & Özdemir, 1997). This is illustrated in a Day diagram in Figure 5b for crushed magnetite samples that were measured before and after annealing (from Dunlop, 2002a). Hysteresis data for the annealed samples are indicative of "coarser" magnetite compared to the stressed, unannealed samples.

Internal stress controls domain state in titanomagnetite (Appel, 1987; Appel & Soffel, 1984, 1985; Halgedahl, 1987). Appel (1987) estimated the average internal stress in variably oxidized titanomagnetite ($x \approx 0.6$) to be between 27 and 63 MPa, with a mean of 48 MPa. Lattice distortions due to low-temperature oxidation could be a key contributor to internal stress (Appel, 1987; Petersen & Vali, 1987), as discussed in section 2.5. Özdemir

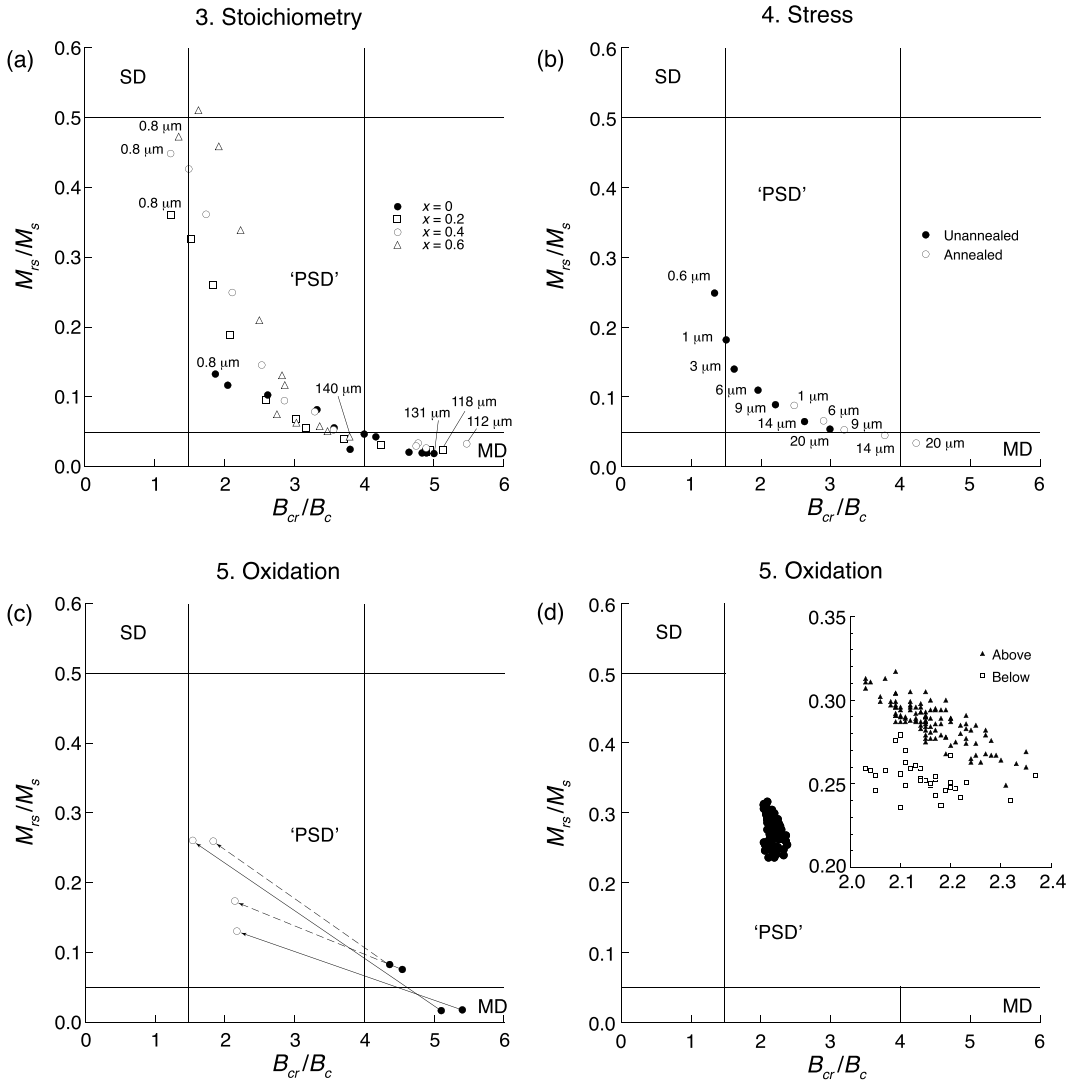

Figure 5. Illustration of the effects of titanomagnetite stoichiometry, stress, and oxidation on data distributions in a Day diagram. (a) Illustration of the effect of titanomagnetite stoichiometry for the same Day diagram as shown in Figure 1c, but with different symbols used to denote different Ti contents (x) in the four titanomagnetite sample series analyzed by Day et al. (1977). Particles with 0.8 μm size span almost the entire data range from SD to MD for x = 0–0.6, and a ~30 μm size range has similar M_{rs}/M_s values for variable x values. (b) Illustration of the effect of stress on data distributions in Day diagrams for crushed natural magnetite samples before (black circles) and after (open circles) annealing (from Dunlop, 2002a). (c, d) Illustration of the effect of magnetite oxidation on data distributions in Day diagrams for: (c) natural magnetite samples before (black circles) and after (open circles) low-temperature oxidation, where pairs of data are joined by arrows (from Cui et al., 1994; Özdemir & Dunlop, 2010), and (d) surface sediments from Ontong-Java Plateau above and below the diagenetic Fe-reduction front (from Tarduno et al., 1998; Smirnov & Tarduno, 2000). See text for details.

and Dunlop (1997) observed bowing of domain walls in magnetite and interpreted it as tangible evidence of the effect of internal stresses on domain structure and calculated internal stress values of 7–34 MPa. These internal stress levels are similar to those encountered at moderate geological burial depths, where lithostatic pressures of 25 and 100 MPa are equivalent to burial at 1 and 4 km, respectively. Gilder (2007) summarized the considerable effects of pressure on magnetic properties, including demagnetization and hardening of coercivity, which are pertinent to hysteresis parameter interpretation.

The state of stress of constituent magnetic minerals is almost always unknown in bulk geological samples. Also, different magnetic particle fractions in a sample could have different states of internal stress. For example, titanomagnetite forms in igneous bodies under variable temperatures and pressures. Materials from

deep sources are likely to have been subjected to decompression with uplift to the surface; after being liberated from the host rock titanomagnetite will experience abrasion during erosion and transportation, and subsequent pressurization during postdepositional burial. Regardless of their history and journey, it would be surprising for such particles to be stress free. Even if stress is avoided during these processes, exposure of (titano) magnetite to the atmosphere for prolonged time periods will cause surface oxidation, which will produce intraparticle stress, as discussed below. Biogenic and pedogenic magnetite, in contrast, form via organically controlled or inorganic mineralization from ions in solution in natural environments and are not expected to be highly stressed. Maher (1988) argued that her pure synthetic stoichiometric magnetite samples are structurally unstressed and represent close analogs of those found in soils and sediments. Thus, incorporation of detrital and biogenic or pedogenic magnetic particles is likely to involve a combination of stressed and unstressed particles with the respective stresses affecting each component differently (cf. Figure 5b). This situation represents a significant unknown in use of hysteresis parameters for granulometric purposes.

2.5. Surface Oxidation

Magnetite is a mixed valence iron oxide ($Fe^{2+}Fe_2^{3+}O_4$) that is thermodynamically unstable in oxidizing environments. In such environments, oxygen diffuses in and Fe^{2+} migrates out of the spinel lattice to create site vacancies. The resulting core-shell mismatch, where surficial maghemite has a smaller crystal lattice size than the magnetite core (Housden & O'Reilly, 1990; Petersen & Vali, 1987), produces irregular, curved shrinkage cracks on the outer parts of the resulting composite particles (Nowaczyk, 2011; Petersen & Vali, 1987).

It is straightforward to reduce partially oxidized magnetite via heating in a reducing atmosphere, or to oxidize fresh stoichiometric magnetite rapidly via heating in an oxidizing atmosphere (e.g., Özdemir & Dunlop, 2010). This makes it experimentally simple to compare hysteresis results for partially oxidized magnetite compared to reduced stoichiometric magnetite. Despite this, few relevant measurements have been published (e.g., Cui et al., 1994; Özdemir & Dunlop, 2010), as shown in Figure 5c. Data points for fresh stoichiometric magnetite are shown as solid circles, while results for the same partially oxidized material are shown as open circles. Lines with arrows in Figure 5c indicate the respective pairs of data points. The effect of oxidation is large, with M_{rs}/M_s increasing and coercivity becoming significantly harder. With stretching of the partly oxidized maghemite shell over the magnetite core, stress increases due to increased magnetostriction, which increases the coercivity (e.g., Appel, 1987; Beske-Diehl & Soroka, 1984; Housden & O'Reilly, 1990; Knowles, 1981; Smith, 1987). M_s decreases with oxidation, and M_{rs} has been assumed to follow the same trend (e.g., Smith, 1987), although in Figure 5c, M_s has decreased more in proportion to M_{rs} so that M_{rs}/M_s is larger after oxidation. Overall, oxidation causes a significant shift in the position of data for such samples in a Day diagram (Figure 5c).

Tarduno et al. (1998) and Smirnov and Tarduno (2000) provide a natural example of surface oxidation effects on hysteresis parameters for magnetite in marine sediments. SD biogenic magnetite formed within these sediments at shallow depths between the diagenetic Mn- and Fe-reduction fronts (Tarduno & Wilkison, 1996) and was then oxidized surficially as oxygen diffused into the sediment (Smirnov & Tarduno, 2000). As the particles were buried through the Fe-reduction front, their maghemitized surfaces were then dissolved reductively to produce a more stoichiometric magnetite. The coercivity decreased after this surface dissolution, which is consistent with loss of the more highly stressed oxidized surface material. Burial of sediments through the Fe-reduction front produces a marked effect on the measured hysteresis parameters and their distribution on a Day diagram (Figure 5d), which illustrates how oxidation can cause significant changes in hysteresis parameters with respect to stoichiometric magnetite.

Partial oxidation of magnetite is reported commonly in terrestrial eolian deposits (e.g., Liu et al., 2007), in oxic deep-sea sediments (e.g., Chang et al., 2013; Henshaw & Merrill, 1980; Kawamura et al., 2007, 2012; Passier & Dekkers, 2002; Smirnov & Tarduno, 2000; Torii, 1997; Yamazaki et al., 2003), and during incipient weathering of subaerially exposed marine sediments (van Velzen & Zijderveld, 1995). Therefore, it is reasonable to expect that when (titano)magnetite is present in geological samples, it will have at least partially oxidized surfaces. As indicated in Figures 5c and 5d, this can have a substantial effect on hysteresis parameters. But the extent, and any variation in extent, of surface oxidation are likely to remain undetected and represent a significant unknown in typical applications involving Day diagrams. To make matters more complicated, particle size thresholds for different domain states change substantially with low-temperature titanomagnetite

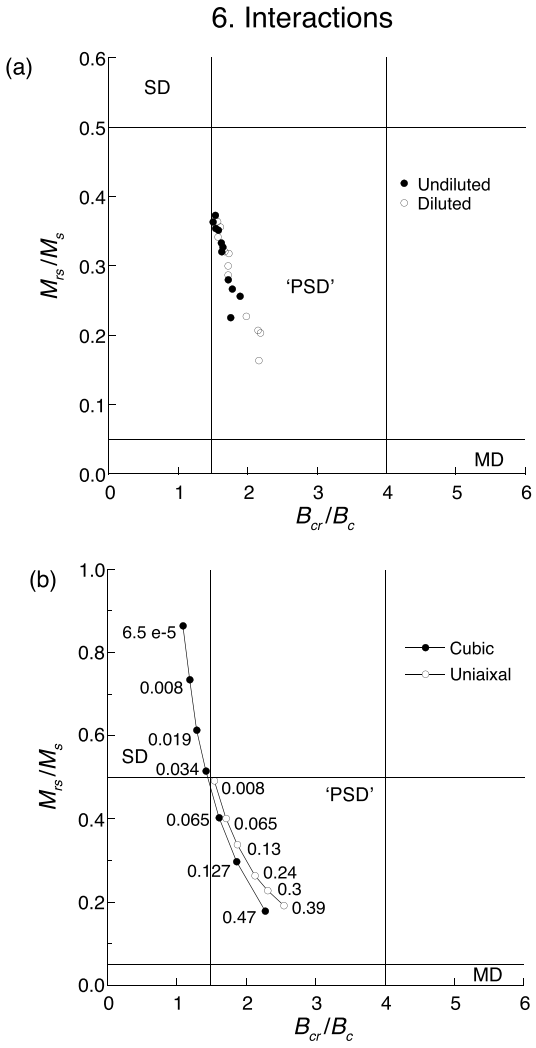

Figure 6. Illustration of magnetostatic interaction effects on data distributions in Day diagrams. Day diagrams for: (a) undiluted and diluted Al-magnetite particles (unpublished results from Jiang et al., 2016) where magnetostatic particle clustering prevented successful sample dilution; and (b) calculated effects of progressively increased interactions represented by the packing fraction p of magnetic particles with either cubic (solid circles) or uniaxial (open circles) anisotropy (from Harrison & Lascu, 2014). See text for details.

oxidation (Moskowitz, 1980). This makes domain state diagnosis from hysteresis measurements precarious when details of mineral oxidation are unknown.

2.6. Magnetostatic Interactions

Day et al. (1977) pointed out that their studied samples were affected by magnetostatic clustering that made it difficult to measure particle size distributions precisely and that affected hysteresis results. They reported no effect of concentration on hysteresis properties for high-Ti titanomagnetite, but increasing magnetite concentrations lowered B_c, B_{cr}, and M_{rs}/M_s. They, therefore, used magnetite concentrations of 1% by weight for their reported experiments. Few studies have quantified magnetostatic interaction effects, which are notoriously difficult to assess and have complicated effects. For example, the compilation in Figure 2 involves different studies and types of samples with variable and unknown contributions from magnetostatic interactions.

We show results for one relevant data set and one set of calculations in Figure 6 to illustrate complexities associated with magnetostatic interactions. Initial hysteresis results for synthetic Al-substituted magnetites of Jiang et al. (2016) were made on nondiluted samples with no attempt to reduce magnetostatic interactions (solid symbols in Figure 6a). Later efforts to disperse the Al-magnetite particles and embed them in paramagnetic CaF_2 cement were partially effective in reducing interactions and produced a greater data spread in a Day diagram (open symbols in Figure 6a). FORC diagrams are useful for quantifying interactions and were measured for both sets of samples. Unsurprisingly, efforts to physically dilute the samples were only partially successful. Magnetostatic interactions are extremely difficult to avoid for synthetic powder samples because magnetic attractions will always cause clumping so that separating particles at the nanometer scale is challenging. Magnetostatic interactions clearly have significant effects on data distributions in Day diagrams (Figure 6a).

Production of regular grids of magnetic particles with controlled stoichiometry, size, and spacing using electron beam lithography (EBL) is a potentially powerful means to resolve these issues and to assess quantitatively the effects of magnetostatic interactions. However, relatively few nonideal samples have been produced (King et al., 1996; Krása et al., 2009), where the samples are often affected by induced stress related to the sample/thin-film-substrate interface. The number of available samples remains too small, and the quality of the samples is too limited to be able to draw firm conclusions. Nevertheless, the ability to produce improved samples in future via EBL should be a significant boon to improving our understanding of the effects of interactions.

Limitations in our ability to quantify the effects of magnetostatic interactions experimentally can be overcome by numerical simulations. Sprowl (1990) made analytical calculations of the effects of increased packing of interacting Stoner and Wohlfarth (1948) particles, Muxworthy et al. (2003) used 3-D micromagnetic simulations to calculate the effects of interactions among magnetic particles with different sizes and anisotropy types, and Harrison and Lascu (2014) calculated the effects of interactions among magnetic particles with different sizes and anisotropy types using a simplified micromagnetic approximation with interacting Stoner and Wohlfarth (1948) particles. Simulated effects of increasing packing density on hysteresis parameters for stable SD particles with either cubic or uniaxial anisotropy from Harrison and Lascu (2014) are illustrated in Figure 6b, where the packing fraction, p, is given by $p = \frac{1}{L^3}\Sigma_{i=1}^{N} V_i$. L is the dimension of the cubic

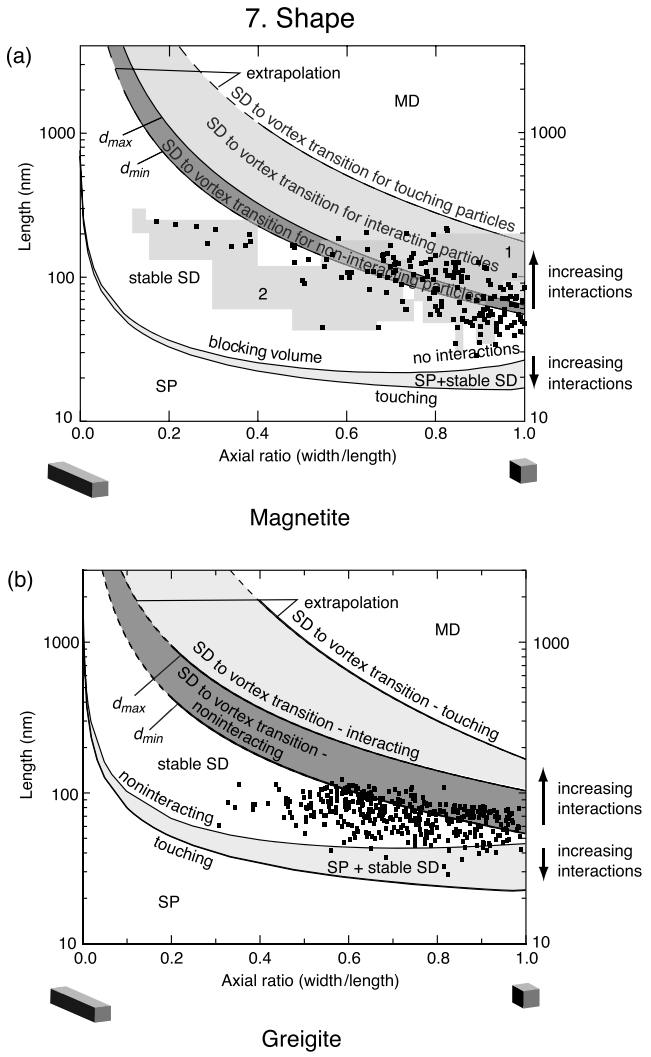

Figure 7. Illustration of the relationship between magnetic particle shape and domain state for magnetite and greigite. For example, elongated 1-μm particles are in the SD state, whereas equant particles with the same length are in the MD state. Domain state phase diagrams for (a) magnetite and (b) greigite are adapted from Muxworthy and Williams (2009) and Muxworthy et al. (2013), respectively. Shaded rectangular data distributions for bacterial magnetosomes in (a) are from Kopp and Kirschvink (2008) and data points are from Larrasoaña et al. (2012). Data distributions for multicellular magnetotactic prokaryotes in (b) are from Pósfai et al. (2001).

space in which the particles are packed randomly, and V is the volume for each particle i from 1 to N. Hysteresis values are as expected for low p but move away from the expected values and toward MD-like values with moderate increases in p (Figure 6b). Bacterial magnetite chain collapse also decreases M_{rs}/M_s (Harrison & Lascu, 2014) to values like those for magnetite magnetofossil-bearing samples in Figure 3a. Such simulations are important because magnetofossil-bearing samples are likely to contain a mixture of *intact* and collapsed chains (Egli et al., 2010). In these simulations, magnetostatic interactions cause SD particles to appear more MD like and provide another source of bias that causes the PSD state to be overrepresented (e.g., Egli & Winklhofer, 2014) with respect to the stable SD state.

Notwithstanding the clarity of the results shown in Figure 6b, understanding magnetostatic interaction effects in magnetic particle assemblages is challenging because they are determined by the interplay between nonlinear, short- and long-range interactions, and thermal fluctuations (Muxworthy, 2013). Numerical simulations reveal nonintuitive complexities (Muxworthy et al., 2003; Muxworthy & Williams, 2005), where interacting SD grains can become more MD-like in character, as illustrated above, and interacting particles in the magnetic vortex state can become more SD like in character by forming supervortex structures. Also, magnetofossil chain collapse can cause flux linking to produce supervortex structures even though individual magnetic particles are in the SD state (Egli & Winklhofer, 2014; Harrison & Lascu, 2014). FORC diagrams are a powerful tool for assessing magnetostatic interactions (Pike et al., 1999; Roberts et al., 2000), but they cannot discriminate between interparticle interactions and intraparticle interactions associated with domain walls. Likewise, they cannot discriminate between vortex states within particles or the supervortex states that can occur when adjacent particles interact magnetically (cf. Egli & Winklhofer, 2014; Harrison et al., 2002). Thus, combined approaches are needed that combine numerical simulations (Muxworthy et al., 2004), magnetic measurements, and electron microscopy or electron holography where mineralogical and/or magnetic structures can be imaged to understand the interactions and how they affect magnetic results. For example, the magnetostatically interacting samples illustrated with FORC diagrams in Figure 4 are explained by the presence of interlocking pyrrhotite plates (Weaver et al., 2002). Overall, magnetostatic interactions have major effects on data distributions in Day diagrams and are a significant source of interpretive uncertainty.

2.7. Particle Shape

As soon as SD particles become slightly nonequant, shape anisotropy overshadows magnetocrystalline anisotropy in controlling the magnetic behavior of strongly magnetic materials such as magnetite, maghemite, and iron (Dunlop & Özdemir, 1997; Tauxe et al., 2002, 2010). Particle shape, therefore, exerts a critical control on domain state threshold sizes. For example, in early domain state phase diagrams produced from analytical calculations (Butler & Banerjee, 1975; Evans & McElhinny, 1969), there was no stable SD state at room temperature in equant magnetite particles. In 3-D micromagnetic simulations (Muxworthy & Williams, 2009; Nagy et al., 2017), the SD state exists for equant magnetite particles at room temperature, but its size range is much smaller than for more elongated particles (Figure 7a). Thus, textbook illustrations of Néel (1949, 1955) theory for stable SD particles in rock magnetism and paleomagnetism usually involve calculations for elongated magnetite particles (e.g., Tauxe et al., 2010, used a 1.3: 1 length: width ratio).

It is difficult to illustrate the effects of shape variations on magnetic properties while holding particle size/volume constant because natural materials rarely meet this condition and we cannot produce synthetic samples with sufficiently controlled particle size or shape or volume. In natural examples such as the Tiva Canyon Tuff, where grain size varies over a narrow range and particle shape is important, hysteresis results are still controlled dominantly by grain size variations (e.g., Till et al., 2011). In contrast, magnetotactic bacteria produce magnetic particles naturally via intracellular biomineralization with variable shape, but with size/shape distributions that lie consistently in the stable SD size range (e.g., Kopp & Kirschvink, 2008). Such magnetosome particles have equidimensional cubo-octahedral, elongate hexaoctahedral prismoidal, and irregular and elongate tooth, bullet (Thornhill et al., 1994), and arrowhead (Bazylinski et al., 1995) morphologies. Particles with these variable morphologies typically co-occur, which makes it difficult to disentangle how any single morphology affects the distribution of parameters on a Day diagram with respect to co-occurring magnetosomes with different morphologies. However, it is possible to compare magnetosome sizes and shapes from transmission electron microscope (TEM) observations with micromagnetic calculations of domain state threshold sizes for particles with varying aspect ratios (Figure 7) for magnetite (Muxworthy & Williams, 2009) and greigite (Muxworthy et al., 2013). Magnetosome morphologies for magnetite have been grouped into cuboidal, elongate prismatic, and elongate irregular categories (Kopp & Kirschvink, 2008), and their data ranges are plotted along with individual data from Larrasoaña et al. (2012) in Figure 7a. Likewise, data distributions for greigite-producing multicellular magnetotactic prokaryotes (Pósfai et al., 2001) are plotted alongside calculated domain state ranges in Figure 7b. From such comparisons of magnetosome shape and micromagnetic calculations, considerable shape variations clearly occur within the SD state. Variable particle morphology is highly probable in natural samples, whether or not they contain fossil magnetosomes. Thus, use of the Day diagram for absolute granulometry is precluded and relative granulometry is complicated by unknown magnetic particle shape variations.

2.8. Thermal Relaxation

The theoretical M_{rs}/M_s value of 0.5 for uniaxial SD particles (Stoner & Wohlfarth, 1948) is based on the assumption that each particle has a constant absolute magnetic moment where the moment rotates coherently with changing applied field. This assumption only holds rigorously at 0 K where thermal energy is zero. At ambient temperatures, thermal fluctuations can cause magnetic moments to relax and follow an ambient field, so that the magnetization decays to approach a thermodynamic equilibrium over time (Brown Jr, 1959, 1963; Néel, 1949, 1955). Such thermally relaxed SP particles do not have a stable remanent magnetization, and M_{rs}, B_c, and B_{cr} of assemblages of such particles are zero. Thus, when part of a SD magnetic mineral assemblage undergoes thermal relaxation, hysteresis values will move away from the SD region of a Day diagram. SD/SP mixtures can cause distorted hysteresis loops, where SP particles lower B_c and M_{rs} to produce lower M_{rs}/M_s values and higher B_{cr}/B_c values (e.g., Jackson, 1990; Nagata & Carleton, 1987; Parry, 1982; Roberts et al., 1995; Tauxe et al., 1996). The effects of thermal relaxation on Day diagram data distributions have been calculated in various ways. Tauxe et al. (1996) used a Langevin function to simulate mixtures of various SP particle sizes with thermally stable SD particles to explain patterns observed in Day diagrams for natural samples. Dunlop (2002a) calculated hysteresis parameters for mixtures of thermally stable SD and SP magnetite end-members, where the SP particles have a single fixed size (rather than representing a size distribution) ranging from 10 to 30 nm to produce the now-famous SD + SP mixing lines discussed in section 2.9. Such singular particle sizes are unlikely to occur in nature but have been invoked to explain features observed in remagnetized Paleozoic limestones (Jackson, 1990; McCabe & Channell, 1994), as discussed below. The SD + SP mixing lines of Dunlop (2002a) lie in the top right-hand region of the Day diagram. If SP particles always have such sizes, they would draw any trend on a Day diagram down and to the right and would not cause serious interpretive ambiguity. Such patterns result directly from the use of a single SP particle size in the mixing model. Rather than treating SD and SP particles as separate end-members, Lanci and Kent (2003) built thermal activation at 300 K into the Stoner and Wohlfarth (1948) model to represent relaxation of part of the magnetic particle assemblage, which provides a more realistic treatment of natural particle size distributions. Using a particle assemblage with a distribution of anisotropies, they produced data trends in a Day diagram that track through the middle of the PSD region (Figure 8) and, therefore, produce considerably greater interpretive ambiguity than the approach of Dunlop (2002a). Heslop (2005) simulated thermal activation in magnetic particles with identical size. While this approach is not geologically realistic, it enables determination of the effects of thermal activation alone without the effects of anisotropy variations. In this case,

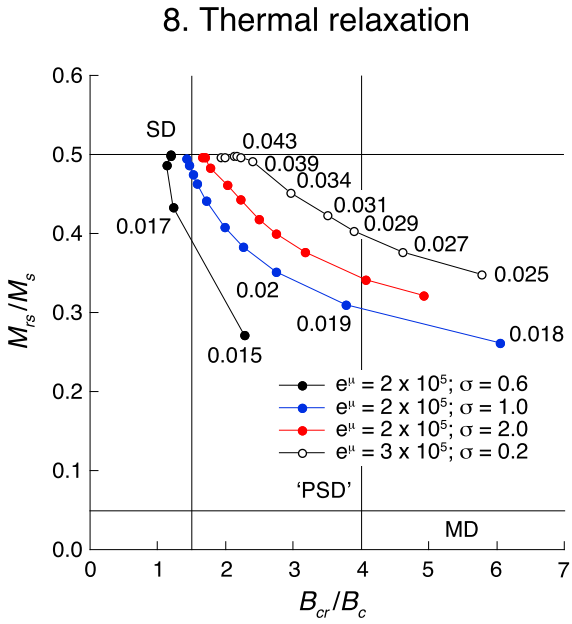

Figure 8. Illustration of thermal relaxation in SD particle systems in a Day diagram. Results are for a thermally activated Stoner and Wohlfarth (1948) model at 300 K for magnetite (Lanci & Kent, 2003), where particle size distributions are approximated by lognormally distributed uniaxial anisotropy constants K_u, where μ is the central point of the distribution and σ is the dispersion (analogous to the Gaussian mean and standard deviation; μ is shown as exp(μ), i.e., the actual mean). B_{cr} is from simulated hysteresis loops following Tauxe et al. (1996). Numbers beside data points indicate equivalent particle sizes (in μm) for cubic particles.

increased thermal activation causes data to move from the stable SD region into the PSD region of a Day diagram following similar trends to the SD + MD mixing lines of Dunlop (2002a). This conclusion is supported by experimental results for mixed stable SD (magnetotactic bacteria) and SP (ferrofluid) particles, where an increased SP component produces a mixing line that passes through the PSD region (Kumari et al., 2015).

Overall, SP particles are normally thought to move data distributions toward the top right-hand side of a Day diagram, but this is not the only way that thermal activation can affect data distributions. The calculations of Lanci and Kent (2003) and Heslop (2005), and the experimental data of Kumari et al. (2015), indicate that interpretive ambiguity in the Day diagram can be produced both by mixing distinct SP and SD end-members and by part of a single particle size distribution undergoing thermal relaxation.

2.9. Mixing of Magnetic Particles With Different Sizes

Day et al. (1977) stated that it is important to establish the effects of mixing of coarse and fine magnetic particles because hysteresis parameters can be influenced differentially by variable concentrations of coexisting hard and soft magnetic fractions. With the ensuing increased use of Day diagrams, it was recognized that natural samples rarely contain a single magnetic component and that mixing is routinely important. Dunlop (2002a), therefore, calculated mixing lines for SD + MD and SD + SP mixtures to constrain interpretation of Day diagrams with illustrated examples from experimental data sets (Dunlop, 2002b). These mixing lines (Figure 9a) are now used so extensively that the Day diagram is often referred to as the Day-Dunlop diagram. We now discuss several issues that affect diagnosis of mixtures in the Day diagram.

2.9.1. Definition of End-Members for Component Mixtures

An important issue to consider in relation to the binary mixing lines of Dunlop (2002a) concerns the parameter values used to define the respective end-members. The trends of SD + MD and SD + SP mixing lines are controlled by the M_{rs}/M_s and B_{cr}/B_c values of the end-members. Dunlop (2002a) fixed the MD end-member at M_{rs}/M_s = 0.02 and B_{cr}/B_c = 5, and the SD end-member at M_{rs}/M_s = 0.5 and B_{cr}/B_c = 1.25. Dunlop and Carter-Stiglitz (2006) later revised these end-member values to B_{cr}/B_c = 1.14 and 4.7 for SD and MD assemblages, respectively. These values have not been adopted widely. As discussed in section 2.10.1, these values are based on theoretical and empirical arguments that do not always define the end-members in a sample. In such cases, data diverge from mixing lines and it becomes more useful to understand why the divergence occurs. Heslop and Roberts (2012a) proposed a solution to this issue where a binary mixing line is calculated by optimizing its fit to measured data. An example of this approach is shown in Figure 9b in relation to linear mixing of SD + SP greigite, where data diverge substantially from mixing lines for magnetite because greigite has cubic anisotropy (Roberts et al., 2011). Many data sets diverge from these mixing lines, which outlines the value of using measured data to define trends in a Day diagram (Heslop & Roberts, 2012a). Nevertheless, deeper issues remain with mixing of magnetic particle populations as discussed below.

2.9.2. Binary Mixing

The effects of mixtures on hysteresis parameters and the Day diagram have been discussed widely (e.g., Carter-Stiglitz et al., 2001; Jackson, 1990; Parry, 1982; Roberts et al., 1995; Tauxe et al., 1996). A key issue for such considerations is whether the magnetic properties of respective components are linearly additive; magnetostatic interactions can violate this assumption (e.g., Carter-Stiglitz et al., 2001; Roberts et al., 1995; Yamazaki & Ioka, 1997). Carter-Stiglitz et al. (2001) considered this issue by analyzing mixed samples in various proportions and concluded that magnetization parameters depend linearly on the mixing ratio, but that coercivity does not. Furthermore, they obtained different lines when mixing different end-members. Dunlop (2002a) used theoretical considerations to develop linear and nonlinear mixing equations for binary SD + MD and SD + SP mixtures and assessed them against data from natural and synthetic samples (Dunlop, 2002a,

2002b). Dunlop and Carter-Stiglitz (2006) then mixed three SD samples with one MD end-member (synthetic Wright magnetite) to test predictions from these equations. In one case (Tiva Canyon Tuff SD end-member), linear mixing theory gave a near-perfect fit to the data. In a second case (glass ceramic SD end-member), linear mixing gave an "unacceptable" fit, and a better but imperfect fit was achieved with a nonlinear mixing equation. In a third case (biogenic SD magnetite end-member), both linear and nonlinear mixing equations failed to fit the data. Dunlop and Carter-Stiglitz (2006), therefore, asked the question "Given the mixed success of our modelling, why use parameter mixing theory at all?" They then pointed to some of the many variables that affect hysteresis parameters, as mentioned above. Their comments are consistent with the thesis of this paper: that there is too much inherent ambiguity in the Day diagram with respect to natural samples to make it diagnostic of domain state in most cases.

Heslop and Roberts (2012b) developed a method to unmix magnetic hysteresis loops. From analysis of many sedimentary sample sets, they found that binary mixing is rare (e.g., Figure 9b; Heslop & Roberts, 2012a) and that most natural sedimentary samples contain multicomponent mixtures with three or more components. An example of failure of binary mixing from Heslop and Roberts (2012a) is given in Figure 9c, where optimized line fits to measured data result in bootstrapped trend lines that diverge substantially from the mixing lines of Dunlop (2002a). These trends have a form that is inconsistent with binary mixing. Such samples are better treated with hysteresis loop unmixing following Heslop and Roberts (2012b), which enables identification of constituent magnetic components (Figure 9d). Given that binary mixing appears to be relatively rare in sedimentary settings, we now consider higher-order mixing.

2.9.3. Higher-Order Mixing

As indicated by Heslop and Roberts (2012b), binary mixing is rare in natural sedimentary samples, which makes it important to consider ternary and higher-order mixing. For ternary mixing, the Day diagram becomes much more ambiguous. We illustrate a distribution of calculated data points for a three end-member scenario (SD + SP + MD) in Figure 9e, where the 100% value for each end-member is color coded. As is the case with the mixing lines of Dunlop (2002a), the positions of end-members in the Day diagram depend on the values chosen. We use the same values as Dunlop (2002a) for the SD and MD end-members and a 10 nm SP component, noting that the 100% point for the SP component is not defined in a Day diagram because M_{rs}, B_c, and B_{cr} are zero, so that the trend on the right-hand side of the diagram asymptotes toward zero M_{rs}/M_s and undefined B_{cr}/B_c. Regardless of this mathematical necessity for the SP component, the overall pattern is clear. As expected, ternary mixing fills the space between the respective vertices for each end-member in the Day diagram. This three-component mixture has a wide range of magnetic properties and spans a large region of the Day diagram, while other mixtures will have less variation and could even fall on an apparent linear trend (e.g., two SD components mixed with a MD component). This demonstrates that ternary and higher-order mixing produces fundamentally ambiguous data distributions in the Day diagram. Given that binary mixing is rare in sedimentary samples and that ternary and higher-order mixing is common, discerning the meaning of data distributions in Day diagrams becomes even more problematical.

We illustrate higher-order mixing with two examples: one from sediments and one from igneous rocks (Figures 9f and 9g). We identify four magnetic components routinely in pelagic carbonates (Roberts, Florindo, et al., 2013) (detrital magnetite, detrital hematite, and the biogenic hard and soft magnetite components of Egli, 2004). These sediments are often almost pure white and weakly magnetic. Three of these components have SD properties (two biogenic magnetite components and hematite), and the detrital magnetite component is coarser grained, so that data lie on a trend that looks like a binary mixing line in a Day diagram (solid black circles in Figure 9f) that lies between the SD + MD and SD + SP mixing lines of Dunlop (2002a). In addition to these data from dominantly biogenic marine sediments (Figure 3a), data from mixed biogenic-terrigenous marine sediments (Figure 3b) and from dominantly terrigenous marine sediments (Figure 3d) fall on a similar trend (Figure 9f). Hysteresis data from basalts (Di Chiara et al., 2014) fall on the same trend (Figure 9g). Intriguingly, this trend for sedimentary and volcanic data falls on a line calculated here for mixtures of MD magnetite and SD particles with cubic anisotropy (for parameters, see Table 1), or the multiaxial anisotropy proposed by Tauxe et al. (2002), rather than on the lines of Dunlop (2002a). Given our comments above about the limitations of mixing lines, we refrain from further comment on the correspondence between measured data and our mixing lines for cubic anisotropy. Data for submarine basaltic glass diverge from the cubic SD + MD trend and toward the region for fine SP particle admixtures, as expected for materials with substantial SP concentrations (Tauxe et al., 1996). These examples illustrate the magnetic

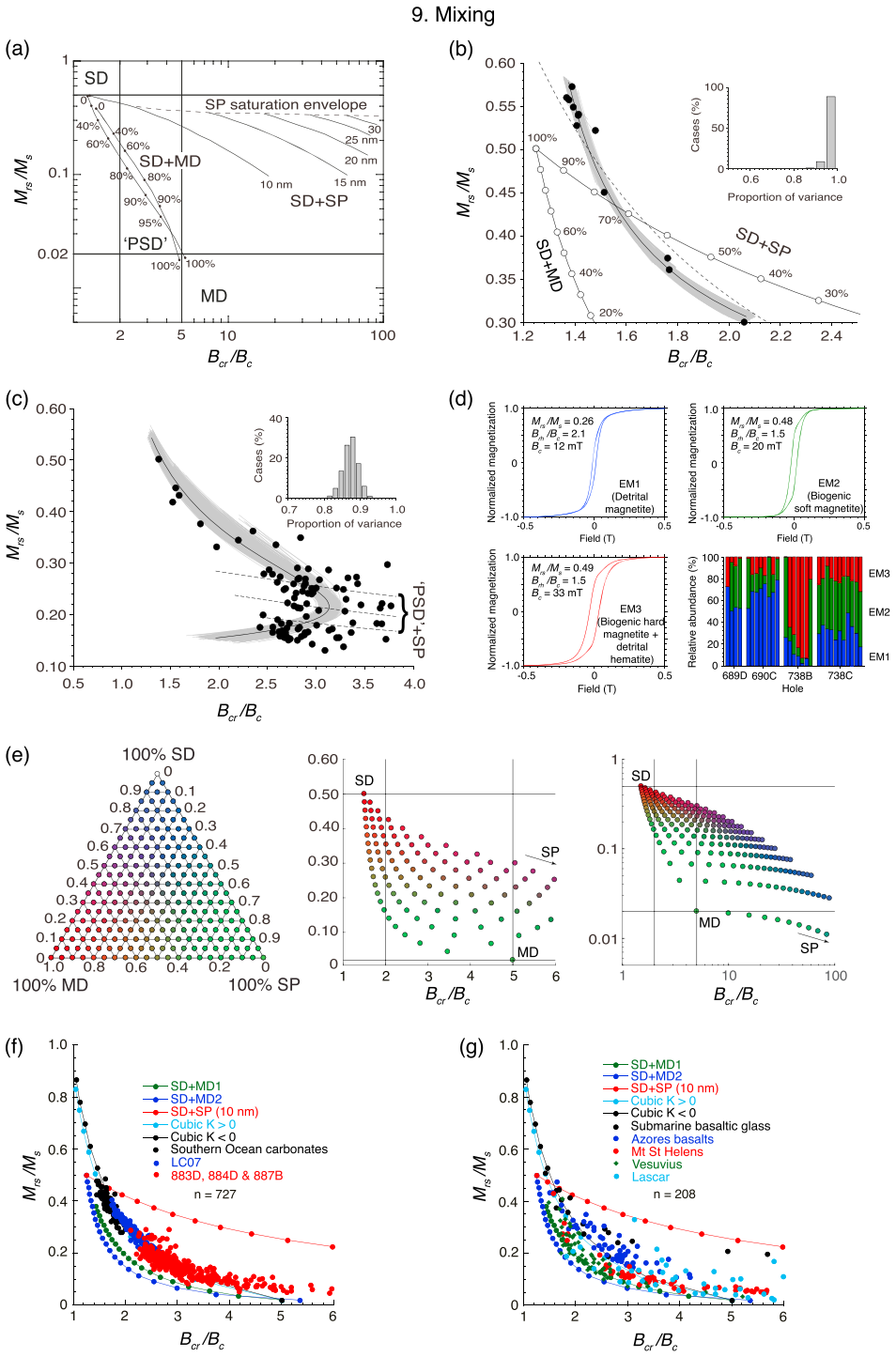

Figure 9. Binary and ternary mixing effects in a Day diagram. (a) Day diagram with binary mixing lines of Dunlop (2002a). (b) Illustration of the method of Heslop and Roberts (2012a) for fitting a data-defined binary mixing line for a SD+SP greigite mixture (black circles: data) (Roberts et al., 2005). The best fit is represented by the black line obtained from 100 bootstrap estimates (gray lines). The data-defined mixing line matches the SD+SP mixing line (dashed) for greigite (Roberts et al., 2011) more closely than for magnetite (Dunlop, 2002a). Data for greigite are offset from the line for magnetite because of the cubic anisotropy of greigite (Roberts et al., 2011). Inset: distribution of the proportional variance of each bootstrap line. (c) Illustration from Heslop and Roberts (2012a) of a data-defined best fit trend for lake sediments (Roberts et al., 1996), which is better fitted with three components (Heslop & Roberts, 2012b). Other features are as in (b). (d) Example of hysteresis unmixing (Heslop & Roberts, 2012b) for pelagic carbonates with concentrations of each identified component in samples from four sequences (Roberts, Florindo, et al., 2013). One of the three end-members is also a mixture (biogenic hard and detrital hematite). (e) Ternary mixing (left) and the respective mixing space in a Day diagram (right) for a SP+SD+MD mixture calculated here. Data distributions for (f) sedimentary and (g) igneous samples (from Figure 3) with SD+MD and SD+SP mixing lines of Dunlop (2002a), and the SD+MD mixing lines calculated here for cubic anisotropy (Table 1).

Table 1
SD+MD Mixing Lines for Cubic Anisotropy

SD end-member: $K_1 > 0$; $M_{rs}/M_s = 0.831$; $B_{cr}/B_c = 1.04$

f_{SD}	B_{cr}/B_c	M_{rs}/M_s
0.0	5.000	0.020
0.1	3.317	0.101
0.2	2.554	0.182
0.3	2.103	0.263
0.4	1.801	0.344
0.5	1.586	0.426
0.6	1.423	0.507
0.7	1.296	0.588
0.8	1.194	0.669
0.9	1.110	0.750
1.0	1.040	0.831

SD end-member: $K_1 < 0$; $M_{rs}/M_s = 0.866$; $B_{cr}/B_c = 1.08$

f_{SD}	B_{cr}/B_c	M_{rs}/M_s
0.0	5.000	0.020
0.1	3.440	0.105
0.2	2.661	0.189
0.3	2.191	0.274
0.4	1.876	0.358
0.5	1.650	0.443
0.6	1.480	0.528
0.7	1.347	0.612
0.8	1.240	0.697
0.9	1.153	0.781
1.0	1.080	0.866

Note. Parameters for SD particles with cubic anisotropy are from Joffe and Heuberger (1974). Parameters for the MD end-member are from Dunlop (2002a). f_{SD} is the fraction of the SD component. Mixing lines were calculated using the equations of Dunlop (2002a).

complexity of geological samples and the lack of diagnostic power provided by binary mixing lines for understanding data distributions in Day diagrams.

2.10. Other Issues That Can Affect Data Distributions in Day Diagrams

2.10.1. Definition of Domain State Regions in the Day Diagram

A widely underappreciated issue that is pertinent to the intended aim of diagnosing domain state with Day diagrams relates to definition of the limits of regions attributed to SD, PSD, and MD behavior. These limits (Figure 10a) are defined based on theoretical, empirical, and practical arguments. The SD/PSD boundary at $M_{rs}/M_s = 0.5$ is based on Stoner and Wohlfarth (1948) theory for uniaxial SD particles. However, the B_{cr}/B_c limit for the SD/PSD boundary was set arbitrarily by Day et al. (1977) at 1.5 rather than at 1.09 as in Wohlfarth (1958) to allow for the fact that magnetic mineral assemblages in geological samples have distributed particle sizes (Dunlop, 2002a). Based on various theoretical and empirical arguments, Dunlop (2002a) used boundary values of $M_{rs}/M_s = 0.5$ and $B_{cr}/B_c = 2$ for the SD/PSD boundary and values of $M_{rs}/M_s = 0.5$ and $B_{cr}/B_c = 1.25$ for the SD end-member in mixing lines. Dunlop and Carter-Stiglitz (2006) then revised the end-member B_{cr}/B_c values for SD and MD assemblages to 1.14 and 4.7, respectively. As discussed in section 2.2, the $M_{rs}/M_s = 0.5$ limit is only valid if SD particles are uniaxial. This approach ignores the fact that multiaxial anisotropy controls the magnetization of an important range of minerals. There is strong justification for a dominant multiaxial anisotropy in MORB (Gee & Kent, 1995, 1999; Mitra et al., 2011), which is a globally important rock type. The results of Mitra et al. (2011) might indicate that multiaxial anisotropy is dominant in igneous rocks, although this remains to be demonstrated widely. For example, Lanci (2010) concluded that both uniaxial and multiaxial anisotropies exist in igneous rocks. FORC diagrams can be used to identify multiaxial anisotropy (Harrison & Lascu, 2014), which explains features observed for hematite (Brownlee et al., 2011; Carvallo et al., 2006; Jovane et al., 2011; Muxworthy et al., 2005), monoclinic pyrrhotite (Larrasoaña et al., 2007; Roberts et al., 2010; Weaver et al., 2002; Wehland et al., 2005), and monoclinic magnetite below the Verwey transition temperature at low applied fields (Smirnov, 2007). Variable magnetocrystalline anisotropy type means that the limits for different domain states will vary in the Day diagram. While it is true that the Day diagram was not designed with other minerals in mind, it was designed for titanomagnetite for which the evidence suggests that multiaxial anisotropy is dominant (Gee & Kent, 1995; Mitra et al., 2011).

There is much debate as to where "PSD" behavior stops and true MD behavior begins (e.g., Dunlop & Özdemir, 1997; Heider et al., 1996) even though it is acknowledged to correspond to the point at which the magnetization is controlled by the response of domains and domain walls to the internal demagnetizing field $-NM$, where N is the demagnetizing factor (Dunlop, 2002a; Néel, 1955). Expected M_{rs}/M_s values for MD particles are calculated from $M_{rs} = B_c/N$ (Dunlop, 2002a; Néel, 1955). Different minerals have different values of B_c and M_s, so the MD limit will vary from mineral to mineral, and with stoichiometry. For magnetite, Dunlop (2002a) determined values of $M_{rs}/M_s = 0.02$ and $B_{cr}/B_c = 5$ for the PSD to MD boundary compared to the values of $M_{rs}/M_s = 0.1$ and $B_{cr}/B_c = 4$ used by Day et al. (1977). The lack of a firm basis for defining the parameter limits for different domain states (Figure 10a), and their variation with mineralogy and stoichiometry, adds further uncertainty to use of the Day diagram for domain state diagnosis.

2.10.2. Approach to Saturation

An important factor that can affect experimental estimates of M_{rs}, M_s, and B_{cr}, and, therefore, the position of data on a Day diagram, relates to high-field slope correction of hysteresis loops and the so-called approach to saturation. For example, the approach to saturation has been a significant factor in the debate about whether MORB has uniaxial or multiaxial anisotropy (e.g., Fabian, 2006, 2012; Gee & Kent, 1995, 1999; Mitra et al., 2011,

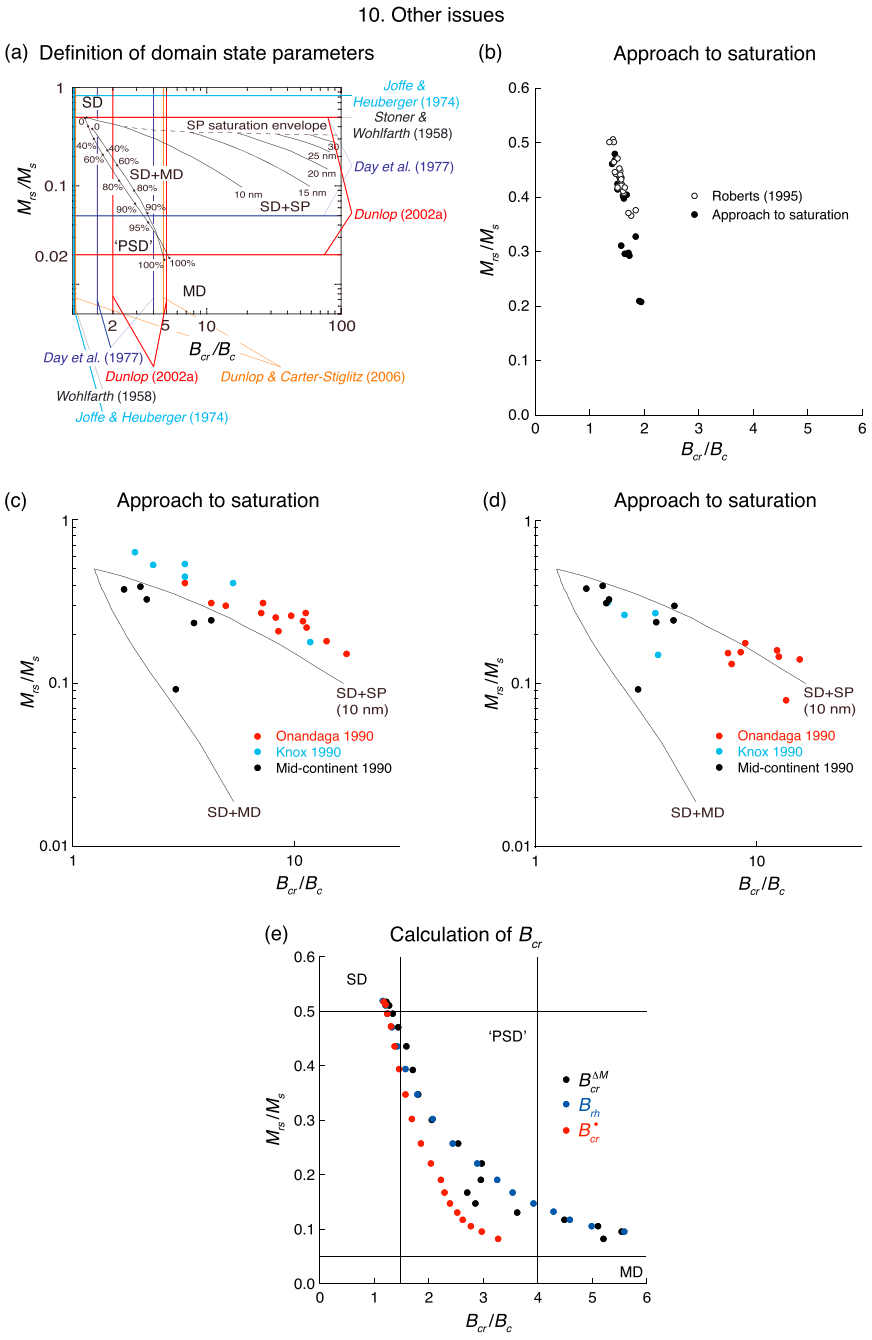

Figure 10. Illustration of other (definitional/experimental) issues that affect data distributions in Day diagrams. (a) Various definitions of regions that demarcate domain states in the Day diagram. Different colors are used to indicate the SD, "PSD," and MD regions defined by Day et al. (1977), Dunlop (2002a), and Dunlop and Carter-Stiglitz (2006), and the SD/"PSD" limits for uniaxial anisotropy from Stoner and Wohlfarth (1948) and Wohlfarth (1958) and for cubic anisotropy from Joffe and Heuberger (1974). (b) Illustration of the effects of variable hysteresis slope correction on Day diagram data distributions. Results from Roberts (1995) (open circles) are for high-field slope corrections from 700 mT to 1 T compared with approach to saturation fits (black circles). Conventional corrections based on M at 70–100% of the maximum applied field gives lower M_{rs}/M_s values than the approach to saturation estimation. (c, d) Comparison for remagnetized Paleozoic carbonates with (c) conventional slope correction (Jackson, 1990), and (d) approach to saturation corrections (Jackson & Swanson-Hysell, 2012). (e) Illustration of the effects on a Day diagram of three B_{cr} estimates obtained directly from hysteresis loops for Monte Carlo simulations of progressive thermal relaxation in SD particle systems (Heslop, 2005). $B_{cr}^{\Delta M}$ is obtained from the difference between ascending and descending hysteresis loop branches, where the $\delta\Delta M/\delta B$ maximum is used to represent B_{cr} (Tauxe et al., 1996). B_{rh} is the median destructive field of the remanent magnetization of the hysteresis loop M_{rh}: $M_{rh}(B) = \frac{M^+(B) - M^-(B)}{2}$, where $M^+(B)$ and $M^-(B)$ are the upper and lower hysteresis loop branches. B_{rh} is consistently higher than B_{cr} from backfield curves (Fabian & von Dobeneck, 1997). If a sample is saturated at $+B_{sat}$, the field can be reduced to zero and then swept back to $+B_{sat}$ to produce a saturation initial magnetization curve M_{si}. B_{cr} is then estimated by comparing the M_{si} curve with $M^-(B)$ and M_{rs} so that $M_{si}(B_{cr}) = M^-(B_{cr}) + M_{rs}$ (Fabian & von Dobeneck, 1997). These issues can be avoided by direct B_{cr} measurement from backfield demagnetization curves. In this paper, results are shown for direct B_{cr} determination, except for Figure 9d where only hysteresis loops are considered and B_{rh} is used.

2012). Hysteresis loops consist of two parts. In the irreversible part, the upper and lower branches are separated (at lower fields), and in the reversible part (at higher fields) both branches coincide. In the reversible part, the magnetization continues to increase due to rotation of magnetic moments parallel to the applied field, which is resisted by the anisotropy of the material. This reversible region is referred to as the approach to saturation. Various mathematical formulations exist for the law of approach to saturation (e.g., Bertotti, 1998; Chikazumi, 1997); Fabian (2006) used the following expression: $M(B) = M_s + \chi B + \alpha B^{\beta}$, where M is the magnetization, B is the field, χ is the susceptibility of all diamagnetic and paramagnetic components, and the final term represents an individual approach to saturation law where both α and β must be negative so that the approach is from below and vanishes for $B \rightarrow \infty$. Use of the law of approach to saturation for geological materials is not straightforward because α and β vary from material to material and must be approximated (e.g., Fabian, 2006; von Dobeneck, 1996). Determination of these parameters is problematical for samples with mixed magnetic components, and robust estimation of approach to saturation is difficult (Jackson & Solheid, 2010). Hysteresis loops can be fitted and extrapolated to high fields to estimate the approach to saturation using hyperbolic functions (Jackson & Solheid, 2010; von Dobeneck, 1996). This method contrasts with the routine correction of hysteresis loops using linear slopes at 70–100% of the maximum applied field, the validity of which depends on whether the magnetization is saturated at 70% of the maximum applied field. We compare the effects of linear slope correction at 70–100% of the maximum applied field (1 T) with estimates from approach to saturation fitting for greigite samples in Figure 10b. In all cases, the conventional slope correction overestimates M_{rs}/M_s compared to the approach to saturation estimation. A similar assessment for remagnetized Paleozoic carbonates by Jackson and Swanson-Hysell (2012) found that results of published hysteresis slope corrections were affected by undersaturation (which affects B_c and M_{rs}/M_s determinations; Figures 10c and 10d). Previous measurements of Jackson (1990) were made to maximum fields of 1 T, 500 mT, or even 300 mT. Such maximum fields are used relatively commonly, which suggests that hysteresis loop undersaturation is likely to be widespread in rock magnetic studies and that inadequate slope correction probably causes an additional large uncertainty for data distributions in the Day diagram.

2.10.3. B_{cr} Estimation

Three of the parameters used in Day diagrams are estimated directly from a hysteresis loop (M_{rs}, M_s, and B_c), while the fourth (B_{cr}) is estimated from a backfield demagnetization curve (Figures 1a and 1b). Fabian and von Dobeneck (1997) summarized three alternative approaches to determine B_{cr} directly from a hysteresis loop. These alternatives give similar but not identical values to B_{cr}. In this paper, we use B_{cr} determinations from backfield curves measured along with hysteresis loops on the same system (Princeton Measurements Corporation Micromag systems in all cases). We consider this approach to be the simplest way to determine B_{cr} because it complies directly with the definition for this parameter and the measurement is made directly with the same instrument settings (although usually with a higher sensitivity setting for remanence compared to in-field measurements). Nevertheless, other approaches for determining B_{cr} exist and will produce different data distributions in a Day diagram. Heslop (2005) calculated such differences from numerical simulations of thermally relaxing magnetic particle systems (Figure 10e). The differences among B_{cr} estimations are significant, which adds uncertainty to Day diagram interpretation. This uncertainty can be avoided by ensuring that B_{cr} is measured directly and consistently from backfield demagnetization curves rather than being estimated from hysteresis loops. As indicated in Figure 2, B_{cr} and B_c both vary with particle size, so that B_{cr}/B_c masks important coercivity information. This led Tauxe et al. (2002) to prefer plots of M_{rs}/M_s versus B_c as used by Néel (1955). This avoids the need to determine B_{cr} and removes ambiguities associated with the fact that both B_c and B_{cr} have particle size dependence (Figure 2). Space prevents us from expanding on the relative merits of the Day and Néel diagrams.

3. Discussion

3.1. Is the Day Diagram Useful?

Our synthesis of experimental results, numerical simulations, and definitional/technical issues indicates that each of the 10 factors discussed above can cause major variations in the position of data on a Day diagram. Most of these factors are unknowns in studies of geological materials. This fundamental ambiguity undermines use of the Day diagram as a tool for diagnosing domain state, particle size, or mineralogy. We urge users of the Day diagram to consider whether their data are sufficiently constrained to enable its

defensible use. We argue that, without considerable additional data, the ambiguities outlined in this paper are usually so debilitating that the Day diagram does not provide the desired domain state diagnosis.

3.2. In What Situations Is a Day Diagram Useful?

If the Day diagram is so ambiguous, it is reasonable to ask "Are there situations in which the Day diagram is useful?" Surely the Day diagram would not be used so widely if it provides no diagnostically useful information? We have used the Day diagram extensively, so we illustrate these questions mainly with our own published examples.

The main benefits of the Day diagram are generally considered to be in assessing relative granulometric variations and paleomagnetic recording efficiency. Concerning relative granulometry, data from marine sediment core LC07 in Figure 3b appear to fall on a mixing line between relatively fine and coarse end-members. Dinarès-Turell et al. (2003) compared these results to $\delta^{18}O$ data from the same core and undertook TEM observations of magnetic mineral extracts to constrain their interpretations. They interpreted data from "coarser" regions in the Day diagram to be caused by increased eolian dust concentrations during glacials and those in "finer" regions to increased SD magnetite magnetofossil concentrations during interglacials. The data fall on a similar trend to those for other sediments (Figure 9f) and not on the SD + MD mixing lines of Dunlop (2002a). Such trends can give the appearance of binary mixing in a Day diagram even though they commonly result from four components (e.g., Roberts, Florindo, et al., 2013). Dinarès-Turell et al. (2003) emphasized two components, but they documented a significant additional hematite component and did not distinguish between the biogenic hard and soft components of Egli (2004). Thus, their data do not represent a binary mixing system. Nevertheless, the overall interpretation of glacial-interglacial magnetic variations in core LC07, which are observed in a range of other magnetic parameters, is robust. Dinarès-Turell et al. (2003) avoided overinterpretation of fine-scale changes in granulometric terms and emphasized relative variations in component mixing. Importantly, the Day diagram was one of several tools used by Dinarès-Turell et al. (2003) to understand environmental controls on magnetic mineralogical trends in core LC07.

Concerning assessment of relative paleomagnetic recording efficiency, it would generally be argued from the trend in Figure 3b, for example, that a sample with $M_{rs}/M_s = 0.4$ will be a more efficient recorder than a sample with $M_{rs}/M_s = 0.2$. The high M_{rs}/M_s value for the former sample would almost certainly be taken to indicate a significant SD particle concentration. Literal interpretation of such a sample as containing dominantly PSD particles would be incorrect, and this pitfall would be avoided by most researchers. In the illustrated case, though, the sample with $M_{rs}/M_s = 0.4$ is not a better recorder; it simply contains a greater concentration of SD magnetite magnetofossils than the sample with $M_{rs}/M_s = 0.2$. Based on analysis of stepwise demagnetization data from this sediment core, virtually all samples (apart from those through polarity transitions) have near-perfect linear demagnetization trajectories (Dinarès-Turell et al., 2002). Thus, it appears that relative concentration differences of coarse and SD components in core LC07 are insufficient to cause differential paleomagnetic directional recording quality. Despite the excellent directional recording, the relative paleointensity signal extracted from this core does not agree well with global stacks (e.g., Valet et al., 2005; Ziegler et al., 2011) through the time period analyzed by Dinarès-Turell et al. (2002). This could be due to differential efficiency of relative paleointensity recording by biogenic and detrital magnetic particles (Roberts et al., 2012), as documented by Ouyang et al. (2014) and Chen et al. (2017). In summary, meaningful information can be extracted from a Day diagram if sufficient additional constraints are obtained and effort is expended to understand the origin of the signals. However, interpretation of the Day diagram in Figure 3b in terms of expected relative paleomagnetic recording would be incorrect.

One of the apparent triumphs of the Day diagram has been in distinguishing between remagnetized limestones and those that retain a primary magnetization (e.g., Channell & McCabe, 1994; Jackson, 1990; McCabe & Channell, 1994). Data distributions for remagnetized carbonates fall largely in a region of the Day diagram that is distinct from those for other geological materials, including carbonates with primary magnetizations (Figure 11a) (see review by Jackson & Swanson-Hysell, 2012). In these remagnetized samples SP particles often contribute ~75% of the total magnetite content (Jackson & Swanson-Hysell, 2012) and give rise to wasp-waisted hysteresis loops that are due in this case to the strongly contrasting coercivities of SP and SD particles (Jackson, 1990; Roberts et al., 1995; Tauxe et al., 1996). These properties are responsible for the distribution of data points on the top right-hand side of the Day diagram. Jackson and Swanson-Hysell (2012) urged caution in using such data distributions in Day diagrams to diagnose

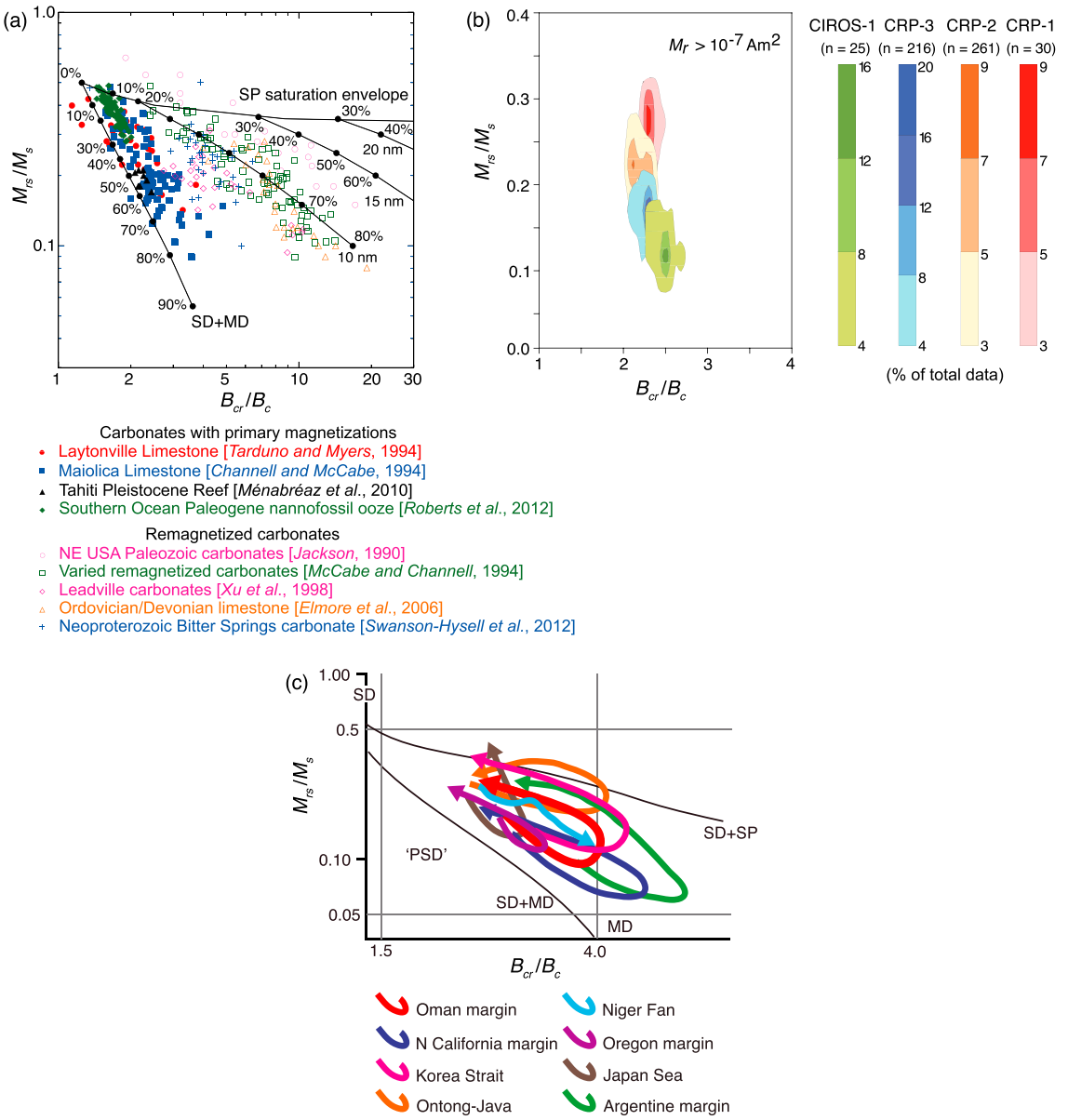

Figure 11. Examples where Day diagrams have proven to be useful. (a) Illustration of contrasting magnetic properties between remagnetized carbonates (open symbols) and those with primary magnetizations (solid symbols). Results are from Jackson (1990), Channell and McCabe (1994), McCabe and Channell (1994), Tarduno and Myers (1994), Xu et al. (1998), Elmore et al. (2006), Ménabréaz et al. (2010), Roberts et al. (2012), and Swanson-Hysell et al. (2012). See Jackson and Swanson-Hysell (2012) for details. (b) Illustration of progressive M_{rs}/M_s increase with decreasing age in Victoria Land Basin, Antarctica (Roberts, Sagnotti, et al., 2013). The overall trend is evident in both weakly and strongly magnetized samples; we show data for $M_{rs} > 10^{-7}$ Am^2, where the % of total data represents a subset of the total data set. (c) Illustration of the effects of down-core reductive diagenesis in shallow marine sediments (Rowan et al., 2009). See text for discussion. Counterclockwise looping trends in hysteresis data have been observed in sediments from the Oman and northern California margins (Rowan et al., 2009), Korea Strait (Liu et al., 2004), Ontong-Java Plateau (Tarduno, 1994, 1995), Niger Fan (Dillon & Bleil, 2006), Oregon margin (Karlin, 1990), Japan Sea (Yamazaki et al., 2003), and Argentine margin (Garming et al., 2005).

remagnetization because of the potential for false positives and false negatives and because it would be surprising for a rock magnetic signature for remagnetization to be generally applicable. They could not cite any cases of false positives (where the Day diagram signature occurs in nonremagnetized carbonates); false negatives are more common but are infrequent (where remagnetized carbonates have signatures typical of nonremagnetized carbonates). Thus, while the Day diagram is an apparent triumph for diagnosing carbonate remagnetization, Jackson and Swanson-Hysell (2012) urge caution in using it for this purpose.

In a study of long-term variations of glacial and volcaniclastic detritus delivered to the Ross Sea, Antarctica, Roberts, Sagnotti, et al. (2013) analyzed hysteresis data for >2,000 samples through a 2.6 km stratigraphic sequence that spans 17 million years (Figure 3c). These data almost all fall in the PSD region of the Day diagram and are distributed widely in the region between the SD + MD and SD + SP mixing lines of Dunlop (2002a). The data fall within a relatively narrow B_{cr}/B_c range, while M_{rs}/M_s increases with decreasing age (the analyzed cores progress from older to younger in the order: CIROS-1 (lower), CRP-3, CRP-2/2A, CRP-1). Roberts, Sagnotti, et al. (2013) used data from the most strongly magnetized samples from each core and contoured their respective distributions in a Day diagram, which demonstrates a progressive M_{rs}/M_s increase with decreasing age (Figure 11b). They interpreted this trend, with assistance from other data types, as reflective of upward fining of the overall magnetic particle assemblage due to increased glacial grinding of source rocks and a greater contribution of volcanic glass from younger McMurdo Volcanic group rocks. In this example, hysteresis data provide useful information despite the data set being large and scattered. Nevertheless, it is a complex, multicomponent data set and it would be risky to undertake deeper analysis of data trends in such a Day diagram without substantial additional constraints. While these data appear to reveal relative particle size variations, they do not reveal whether the magnetic particle assemblages are in the PSD state or the type of component mixing involved.

Finally, we illustrate use of the Day diagram to assess down-core diagenetic changes in marine sediments. Rowan et al. (2009) identified systematic trends in Day diagrams in a sediment core from the Oman margin and from around the world during progressive diagenetic change (Figure 11c). Unaltered detrital magnetic mineral assemblages in surface sediments are subjected to progressive down-core reductive dissolution where the finest particles dissolve to leave a coarser assemblage. With ongoing sulfidization, SP greigite nucleates and its particle size distribution grows progressively into the stable SD size range. This data progression produces a counterclockwise looping trend in Day diagrams (Figure 11c). The trend results from magnetic property contrasts between coarse detrital magnetite, and authigenic SP and SD greigite. Data trends in such Day diagrams are illustrative of processes of interest, although this example has little to do with PSD magnetic behavior even though most of the data fall in the PSD region, and the type of mixing involved does not correspond to that in the mixing lines of Dunlop (2002a).

The cases from Rowan et al. (2009) and Roberts, Sagnotti, et al. (2013) both involve significant SP concentrations that cause data to overlap into the region associated with remagnetized carbonates (compare Figures 3c, 11a, and 11c), although neither case involves carbonates. This observation is consistent with the statement of Jackson and Swanson-Hysell (2012) that it would be surprising for a rock magnetic signature associated with remagnetization to be generally applicable.

3.3. Do Most Magnetic Particles Occur in the PSD State?

The key supposed virtue of the Day diagram is its utility for magnetic domain state diagnosis. As illustrated in Figure 3 for thousands of sedimentary and igneous samples ($n > 3{,}300$), most data fall in the PSD region of the Day diagram. Although it is recognized widely that such designations should not be accepted at face value, a direct result of the dominance of the Day diagram for domain state diagnosis in rock magnetism is that the PSD state is considered widely to be the dominant domain state and that SD particles are relatively rare in geological materials. It is important to ask whether these interpretations are correct.

In this paper, we use the same language as Day et al. (1977) in referring to the SD, PSD, and MD states. We use inverted commas in reference to the PSD state because we consider the term PSD to be a misnomer because it does not represent SD-like behavior (Roberts et al., 2017; Tauxe et al., 2002). PSD behavior is better explained by phenomena associated with single and multiple magnetic vortices, antivortices, and domain walls (Roberts et al., 2017). Tauxe et al. (2010) argued that pseudo multidomain is a better term to describe the PSD state.

Despite this nomenclatural issue, a key observation is that when stable SD particles co-occur with significant quantities of SP, PSD, or MD particles, the M_{rs}/M_s value will decrease, which makes it difficult for an assemblage of magnetite particles to have M_{rs}/M_s values close to 0.5. Data representations in Day diagrams have probably biased against recognition of SD particles and have overemphasized the importance of the PSD state in the paleomagnetic record (Roberts et al., 2012; Tauxe et al., 2002, 2010). An exception involves sediments in which the magnetic properties can be dominated by biogenic SD magnetite, including pelagic

carbonates (e.g., Roberts, Florindo, et al., 2013), which often have M_{rs}/M_s values close to 0.5 (Figure 3a). Overall, representation of hysteresis parameters from bulk samples in a Day diagram mitigates against identification of the true domain states in a sample. If this is the case, it raises significant questions—regardless of the perceived value of the Day diagram—as to why such a tool should be used so widely.

3.4. Is There a Suitable Replacement for the Day Diagram?

The popularity and influence of the Day diagram is evident in the fact that Day et al. (1977) has been cited >2,300 times at the time of writing (Google Scholar). This makes it among the most exceptionally cited papers in rock magnetism. Thus, it will only be replaced if users are convinced, based on evidence such as that presented above, that the Day diagram is misleading, incorrect, or counterproductively ambiguous. It is also unlikely to be superseded unless a suitable alternative exists. This makes it worth asking what qualities a replacement must have to be accepted widely. At minimum, a replacement must provide diagnostic information about domain state. If domain state can be diagnosed, many of the factors discussed above become less important (e.g., stress, surface oxidation, and particle shape) because it is the domain state that is being identified rather than the ambiguity created by these variables. A major weakness of the Day diagram is that it is a biplot of two sets of parameters. The four parameters used in a Day diagram represent only part of the information provided by a hysteresis loop and backfield demagnetization curve. If these parameters capture domain state-specific information, they will be suitable for magnetic granulometry. However, as indicated above, the Day diagram is fundamentally ambiguous. Tauxe et al. (2002) proposed the Néel (1955) diagram (M_{rs}/M_s versus B_c) as an alternative. The Néel (1955) diagram involves fewer parameters than the Day diagram, so it still has limited diagnostic capacity for bulk geological samples that contain mixed magnetic particle systems. Realistically, biplots for bulk samples are unlikely to enable component-by-component discrimination of domain state. In recognition of the weakness of biplots, three-dimensional plots have been proposed in which the axes are M_{rs}/M_s, B_c, and B_{cr} (Borradaile & Hamilton, 2003; Borradaile & Lagroix, 2000). In the near future, we plan to present an assessment of leading contenders that may be suitable alternatives to the Day diagram for accurate domain state diagnosis. Use of constraints from physically realistic three-dimensional micromagnetic models can augment such approaches to illuminate responses for different domain states. Without prolonging the present paper, we simply suggest that unmixing of FORC diagrams, as proposed by Lascu et al. (2015), and determination of remanent and transient FORC diagrams (Zhao et al., 2017) are likely to emerge as suitable candidates for diagnosing domain state on a component-by-component basis within geological samples that typically contain mixtures of magnetic mineral components.

4. Conclusions

The Day diagram has been used widely in rock magnetism for domain state diagnosis. While many ambiguities have long been recognized with respect to the Day diagram, these issues have been largely ignored because of its perceived value for assessing hysteresis behavior in relation to magnetic recording capability and relative granulometry. We have outlined 10 sets of issues that make interpretation of the Day diagram ambiguous for domain state diagnosis. These issues include variations in (1) magnetic mineralogy and (2) the associated magnetocrystalline anisotropy type, (3) mineral stoichiometry, (4) internal stress, (5) surface oxidation, (6) magnetostatic interactions, (7) particle shape, (8) thermal relaxation, (9) mixing, and (10) definitional/measurement issues. In most studies, these variables are unknowns and cannot be controlled for, so that hysteresis parameters for single bulk samples are nonunique and any data point in a Day diagram could result from infinite combinations of relevant variables. Therefore, the Day diagram is fundamentally ambiguous for domain state diagnosis.

The Day diagram has also contributed significantly to other prevailing views that we question. For example, the popularity of the Day diagram for magnetic domain state diagnosis has led to the prevalent interpretation that SD particles are comparatively rare in the geological record and that PSD particles dominate the magnetization of geological materials. However, a range of factors such as mixing with SP, PSD, or MD particles, thermal relaxation, and magnetostatic interactions cause data to fall outside the SD region of a Day diagram, and, therefore, biases against recognition of SD behavior when using the Day diagram. Use of FORC diagrams demonstrates that SD particles are far more common than was previously recognized in the geological record (e.g., Roberts et al., 2012). We argue elsewhere that the PSD state should be referred to as the vortex state (Tauxe et al., 2002), which spans a range of magnetic behaviors associated with single

and multiple vortices, antivortices, and domain walls (Roberts et al., 2017), and unstable "hard-aligned" and stable "easy-aligned" single vortex states (Nagy et al., 2017). While Day et al. (1977) used the prevailing PSD terminology coined by Stacey (1961), and probably had no intention of becoming a key reinforcer of the PSD concept, this is what has happened. The diverse processes that act on magnetic particle assemblages to cause data to fall in the PSD region in a Day diagram have contributed to overemphasis of the importance of the PSD state in rock magnetism. Prevalent use of the Day diagram has also worked against diagnosis of the domain states in magnetic mineral assemblages. Calculation of mixing lines by Dunlop (2002a) has further reinforced use of the Day diagram. From analysis of thousands of samples, binary mixing as envisioned by Dunlop (2002a) appears to be rare in geological materials and ternary and higher order mixing is more common (Heslop & Roberts, 2012a, 2012b). This contributes further ambiguity to the Day diagram.

Based on the issues discussed in this paper, we urge users of Day diagrams to consider whether their data are sufficiently constrained to enable its defensible use. While the Day diagram has been used to valuable effect, in most cases the ambiguities outlined in this paper are so debilitating that it is not useful for domain state diagnosis. There is an urgent need to develop and adopt robust domain state diagnostic tools in rock magnetism to avoid the many pitfalls outlined here in relation to the popular Day diagram.

Acknowledgments
This paper was stimulated by a conversation with Andy Biggin at the International Conference on Rock Magnetism at Utrecht, the Netherlands. A. P. R. acknowledges financial support from the Australian Research Council (through grant DP160100805), and L. T. acknowledges support from the U.S. National Science Foundation (through grants EAR-1547263 and PLR-1541285). The data presented in this paper—which we prefer not to be used for plotting Day diagrams—are available from the lead author on request.

References

Appel, E. (1987). Stress anisotropy in Ti-rich titanomagnetites. *Physics of the Earth and Planetary Interiors*, *46*(1-3), 233–240. https://doi.org/10.1016/0031-9201(87)90185-3

Appel, E., & Soffel, H. C. (1984). Model for the domain state of Ti-rich titanomagnetites. *Geophysical Research Letters*, *11*(3), 189–192. https://doi.org/10.1029/GL011i003p00189

Appel, E., & Soffel, H. C. (1985). Domain state of Ti-rich titanomagnetites deduced from domain structure observations and susceptibility measurements. *Journal of Geophysics*, *56*, 121–132.

Banerjee, S. K. (1971). New grain size limits for palaeomagnetic stability in haematite. *Nature Physical Sciences*, *232*(27), 15–16. https://doi.org/10.1038/physci232015a0

Bazylinski, D. A., Frankel, R. B., Heywood, B. R., Mann, S., King, J. W., Donaghay, P. L., & Hanson, A. K. (1995). Controlled biomineralization of magnetite (Fe_3O_4) and greigite (Fe_3S_4) in a magnetotactic bacterium. *Applied and Environmental Microbiology*, *61*(9), 3232–3239.

Bertotti, G. (1998). *Hysteresis in magnetism* (p. 558). London: Academic Press.

Beske-Diehl, S. J., & Soroka, W. L. (1984). Magnetic properties of variably oxidized pillow basalt. *Geophysical Research Letters*, *11*, 225–228.

Borradaile, G. J., & Hamilton, T. (2003). Limestones distinguished by magnetic hysteresis in three-dimensional projections. *Geophysical Research Letters*, *30*(18), 1973. https://doi.org/10.1029/2003GL017892

Borradaile, G. J., & Lagroix, F. (2000). Magnetic characterization using a three-dimensional hysteresis projection, illustrated with a study of limestones. *Geophysical Journal International*, *141*(1), 213–226. https://doi.org/10.1046/j.1365-246X.2000.00066.x

Brown, W. F. Jr. (1959). Relaxational behavior of fine magnetic particles. *Journal of Applied Physics*, *30*(4), S130–S132. https://doi.org/10.1063/1.2185851

Brown, W. F. Jr. (1963). Thermal fluctuations of a single-domain particle. *Physical Review*, *130*(5), 1677–1686. https://doi.org/10.1103/PhysRev.130.1677

Brownlee, S. J., Feinberg, J. M., Kasama, T., Harrison, R. J., Scott, G. R., & Renne, P. R. (2011). Magnetic properties of ilmenite-hematite single crystals from the Ecstall pluton near Prince Rupert, British Columbia. *Geochemistry, Geophysics, Geosystems*, *12*(9), Q07Z29. https://doi.org/10.1029/2011GC003622

Butler, R. F., & Banerjee, S. K. (1975). Single-domain grain size limits for metallic iron. *Journal of Geophysical Research*, *80*(2), 252–259. https://doi.org/10.1029/JB080i002p00252

Carter-Stiglitz, B., Moskowitz, B., & Jackson, M. (2001). Unmixing magnetic assemblages and the magnetic behavior of bimodal mixtures. *Journal of Geophysical Research*, *106*(B11), 26,397–26,411. https://doi.org/10.1029/2001JB000417

Carvallo, C., Muxworthy, A. R., & Dunlop, D. J. (2006). First-order reversal curve (FORC) diagrams of magnetic mixtures: Micromagnetic models and measurements. *Physics of the Earth and Planetary Interiors*, *154*(3-4), 308–322. https://doi.org/10.1016/j.pepi.2005.06.017

Chang, L., Winklhofer, M., Roberts, A. P., Heslop, D., Florindo, F., Dekkers, M. J., et al. (2013). Low-temperature magnetic properties of pelagic carbonates: Oxidation of biogenic magnetite and identification of magnetosome chains. *Journal of Geophysical Research: Solid Earth*, *118*(12), 6049–6065, https://doi.org/10.1002/2013JB010381

Channell, J. E. T., & McCabe, C. (1994). Comparison of magnetic hysteresis parameters of unremagnetized and remagnetized limestones. *Journal of Geophysical Research*, *99*, 4613–4623. https://doi.org/10.1029/93JB02578

Chen, L., Heslop, D., Roberts, A. P., Chang, L., Zhao, X., McGregor, H. V., et al. (2017). Remanence acquisition efficiency in biogenic and detrital magnetite and recording of geomagnetic paleointensity. *Geochemistry, Geophysics, Geosystems*, *18*, 1435–1450. https://doi.org/10.1002/2016GC006753

Chikazumi, S. (1997). *Physics of ferromagnetism* (p. 655). Oxford: Oxford University Press.

Clark, D. A. (1984). Hysteresis properties of sized dispersed monoclinic pyrrhotite grains. *Geophysical Research Letters*, *11*(3), 173–176. https://doi.org/10.1029/GL011i003p00173

Cui, Y., Verosub, K. L., & Roberts, A. P. (1994). The effect of low-temperature oxidation on large multi-domain magnetite. *Geophysical Research Letters*, *21*(9), 757–760. https://doi.org/10.1029/94GL00639

Day, R., Fuller, M., & Schmidt, V. A. (1977). Hysteresis properties of titanomagnetites: Grain-size and compositional dependence. *Physics of the Earth and Planetary Interiors*, *13*(4), 260–267. https://doi.org/10.1016/0031-9201(77)90108-X

Day, R., Halgedahl, S., Steiner, M., Kobayashi, K., Furuta, T., Ishii, T., & Faller, A. (1978). Magnetic properties of basalts from DSDP Leg 49. *Initial Reports of the Deep Sea Drilling Project*, *49*, 781–791.

Dekkers, M. J. (1988). Magnetic properties of natural pyrrhotite. Part I. Behaviour of initial susceptibility and saturation-magnetization related rock-magnetic parameters in a grain-size dependent framework. *Physics of the Earth and Planetary Interiors*, *52*(3-4), 376–393. https://doi.org/10.1016/0031-9201(88)90129-X

Di Chiara, A., Tauxe, L., & Speranza, F. (2014). Paleointensity determination from São Miguel (Azores Archipelago) over the last 3 ka. *Physics of the Earth and Planetary Interiors*, *234*, 1–13. https://doi.org/10.1016/j.pepi.2014.06.008

Dillon, M., & Bleil, U. (2006). Rock magnetic signatures in diagenetically altered sediments from the Niger deep-sea fan. *Journal of Geophysical Research*, *111*, B03105. https://doi.org/10.1029/2004JB003540

Dinarès-Turell, J., Hoogakker, B. A. A., Roberts, A. P., Rohling, E. J., & Sagnotti, L. (2003). Quaternary climatic control of biogenic magnetite production and eolian dust input in cores from the Mediterranean Sea. *Palaeogeography Palaeoclimatology Palaeoecology*, *190*, 195–209. https://doi.org/10.1016/S0031-0182(02)00605-3

Dinarès-Turell, J., Sagnotti, L., & Roberts, A. P. (2002). Relative geomagnetic paleointensity from the Jaramillo subchron to the Matuyama/Brunhes boundary as recorded in a Mediterranean piston core. *Earth and Planetary Science Letters*, *194*(3-4), 327–341. https://doi.org/10.1016/S0012-821X(01)00563-5

Dunlop, D. J. (1971). Magnetic properties of fine-particle hematite. *Annals of Geophysics*, *27*, 269–293.

Dunlop, D. J. (1986). Hysteresis properties of magnetite and their dependence on particle size: A test of pseudo-single-domain remanence models. *Journal of Geophysical Research*, *91*(B9), 9569–9584. https://doi.org/10.1029/JB091iB09p09569

Dunlop, D. J. (2002a). Theory and application of the Day plot (M_{rs}/M_s versus H_{cr}/H_c): 1. Theoretical curves and tests using titanomagnetite data. *Journal of Geophysical Research*, *107*(B3), 2056. https://doi.org/10.1029/2001JB000486

Dunlop, D. J. (2002b). Theory and application of the Day plot (M_{rs}/M_s versus H_{cr}/H_c): 2. Application to data for rocks, sediments, and soils. *Journal of Geophysical Research*, *107*(B3), 2057. https://doi.org/10.1029/2001JB000487

Dunlop, D. J., & Argyle, K. S. (1997). Thermoremanence, anhysteretic remanence and susceptibility of submicron magnetites: Nonlinear field dependence and variation with grain size. *Journal of Geophysical Research*, *102*(B9), 20,199–20,210. https://doi.org/10.1029/97JB00957

Dunlop, D. J., & Carter-Stiglitz, B. (2006). Day plots of mixtures of superparamagnetic, single-domain, pseudosingle-domain, and multidomain magnetites. *Journal of Geophysical Research*, *111*, B12S09. https://doi.org/10.1029/2006JB004499

Dunlop, D. J., & Özdemir, Ö. (1997). *Rock magnetism: Fundamentals and frontiers* (p. 573). Cambridge: Cambridge University Press. https://doi.org/10.1017/CBO9780511612794

Egli, R. (2004). Characterization of individual rock magnetic components by analysis of remanence curves, 1. Unmixing natural sediments. *Studia Geophysica et Geodaetica*, *48*(2), 391–446. https://doi.org/10.1023/B:SGEG.0000020839.45304.6d

Egli, R., Chen, A. P., Winklhofer, M., Kodama, K. P., & Horng, C. S. (2010). Detection of noninteracting single domain particles using first-order reversal curve diagrams. *Geochemistry, Geophysics, Geosystems*, *11*(1), Q01Z11. https://doi.org/10.1029/2009GC002916

Egli, R., & Winklhofer, M. (2014). Recent developments on processing and interpretation aspects of first-order reversal curves (FORC). *Proceedings of Kazan University*, *156*, 14–53.

Elmore, R. D., Foucher, J. L. E., Evans, M., & Lewchuk, M. (2006). Remagnetization of the Tonoloway Formation and the Helderberg Group in the Central Appalachians: Testing the origin of syntilting magnetizations. *Geophysical Journal International*, *166*(3), 1062–1076. https://doi.org/10.1111/j.1365-246X.2006.02875.x

Evans, M. E., & McElhinny, M. W. (1969). An investigation of the origin of stable remanence in magnetite bearing igneous rocks. *Journal of Geomagnetism and Geoelectricity*, *21*(4), 757–773. https://doi.org/10.5636/jgg.21.757

Fabian, K. (2006). Approach to saturation analysis of hysteresis measurements in rock magnetism and evidence for stress dominated magnetic anisotropy in young mid-ocean ridge basalt. *Physics of the Earth and Planetary Interiors*, *154*(3-4), 299–307. https://doi.org/10.1016/j.pepi.2005.06.016

Fabian, K. (2012). Comment on 'Detecting uniaxial single domain grains with a modified IRM technique' by R. Mitra, L. Tauxe and J. S. Gee. *Geophysical Journal International*, *191*(1), 42–45. https://doi.org/10.1111/j.1365-246X.2012.05478.x

Fabian, K., Kirchner, A., Williams, W., Heider, F., Leibl, T., & Huber, A. (1996). Three-dimensional micromagnetic calculations for magnetite using FFT. *Geophysical Journal International*, *124*(1), 89–104. https://doi.org/10.1111/j.1365-246X.1996.tb06354.x

Fabian, K., & von Dobeneck, T. (1997). Isothermal magnetization of samples with stable Preisach function: A survey of hysteresis, remanence, and rock magnetic parameters. *Journal of Geophysical Research*, *102*(B8), 17,659–17,677. https://doi.org/10.1029/97JB01051

Flanders, P. J. (1991). An alternating gradient magnetometer. *Journal of Applied Physics*, *63*, 3940–3945.

Foner, S. (1959). Versatile and sensitive vibrating-sample magnetometer. *The Review of Scientific Instruments*, *30*(7), 548–557. https://doi.org/10.1063/1.1716679

Garming, J. F. L., Bleil, U., & Riedinger, N. (2005). Alteration of magnetic mineralogy at the sulfate-methane transition: Analysis of sediments from the Argentine continental slope. *Physics of the Earth and Planetary Interiors*, *151*(3-4), 290–308. https://doi.org/10.1016/j.pepi.2005.04.001

Gee, J., & Kent, D. V. (1995). Magnetic hysteresis in young mid-ocean ridge basalts: Dominant cubic anisotropy? *Geophysical Research Letters*, *22*(5), 551–554. https://doi.org/10.1029/95GL00263

Gee, J., & Kent, D. V. (1999). Calibration of magnetic granulometric trends in oceanic basalts. *Earth and Planetary Science Letters*, *170*(4), 377–390. https://doi.org/10.1016/S0012-821X(99)00125-9

Gilder, S. A. (2007). Magnetization, piezoremanence and stress demagnetization. In D. Gubbins & E. Herrero-Bervera (Eds.), *Encyclopedia of geomagnetism and paleomagnetism* (pp. 599–603). Dordrecht: Springer. https://doi.org/10.1007/978-1-4020-4423-6_195

Halgedahl, S. L. (1987). Domain pattern observations in rock magnetism: Progress and problems. *Physics of the Earth and Planetary Interiors*, *46*(1-3), 127–163. https://doi.org/10.1016/0031-9201(87)90178-6

Harrison, R. J., Dunin-Borkowski, R. E., & Putnis, A. (2002). Direct imaging of nanoscale magnetic interactions in minerals. *Proceedings of the National Academy of Sciences of the United States of America*, *99*(26), 16,556–16,561. https://doi.org/10.1073pnas.262514499

Harrison, R. J., & Lascu, I. (2014). FORCulator: A micromagnetic tool for simulating first-order reversal curve diagrams. *Geochemistry, Geophysics, Geosystems*, *15*(12), 4671–4691. https://doi.org/10.1002/2014GC005582

Heider, F., Zitzelsberger, A., & Fabian, K. (1996). Magnetic susceptibility and remanent coercive force in grown magnetite crystals from 0.1 μm to 6 mm. *Physics of the Earth and Planetary Interiors*, *93*(3-4), 239–256. https://doi.org/10.1016/0031-9201(95)03071-9

Henshaw, P. C., & Merrill, R. T. (1980). Magnetic and chemical changes in marine sediments. *Reviews of Geophysics and Space Physics*, *18*(2), 483–504. https://doi.org/10.1029/RG018i002p00483

Heslop, D. (2005). A Monte Carlo investigation of the representation of thermally activated single-domain particles within the Day plot. *Studia Geophysica et Geodaetica*, *49*(2), 163–176. https://doi.org/10.1007/s11200-005-0003-7

Heslop, D., & Roberts, A. P. (2012a). Estimating best fit binary mixing lines in the Day plot. *Journal of Geophysical Research*, *117*, B01101. https://doi.org/10.1029/2011JB008787

Heslop, D., & Roberts, A. P. (2012b). A method for unmixing magnetic hysteresis loops. *Journal of Geophysical Research*, *117*, B03103. https://doi.org/10.1029/2011JB008859

Housden, J., & O'Reilly, W. (1990). On the intensity and stability of the natural remanent magnetization of ocean floor basalts. *Physics of the Earth and Planetary Interiors*, *64*(2-4), 261–278. https://doi.org/10.1016/0031-9201(90)90042-V

Hunt, C., Moskowitz, B. M., & Banerjee, S. K. (1995). Magnetic properties of rocks and minerals. In T. J. Ahrens (Ed.), *Rock physics & phase relations: Handbook of physical constants* (Vol. 3, pp. 189–204). Washington DC: American Geophysical Union. https://doi.org/10.1029/RF003p0189

Jackson, M. (1990). Diagenetic sources of stable remanence in remagnetized Paleozoic cratonic carbonates: A rock magnetic study. *Journal of Geophysical Research*, *95*(B3), 2753–2761. https://doi.org/10.1029/JB095iB03p02753

Jackson, M., & Solheid, P. (2010). On the quantitative analysis and evaluation of magnetic hysteresis data. *Geochemistry, Geophysics, Geosystems*, *11*(4), Q04Z15. https://doi.org/10.1029/2009GC002932

Jackson, M., & Swanson-Hysell, N. L. (2012). Rock magnetism of remagnetized carbonate rocks: Another look. *Geological Society, London, Special Publications*, *371*(1), 229–251. https://doi.org/10.1144/SP371.3

Jiang, Z. X., Liu, Q. S., Zhao, X., Roberts, A. P., Heslop, D., Barrón, V., & Torrent, J. (2016). Magnetism of Al-substituted magnetite reduced from Al-hematite. *Journal of Geophysical Research: Solid Earth*, *121*, 4195–4210. https://doi.org/10.1002/2016JB012863

Joffe, I., & Heuberger, R. (1974). Hysteresis properties of distributions of cubic single-domain ferromagnetic particles. *Philosophical Magazine*, *29*(5), 1051–1059. https://doi.org/10.1080/14786437408226590

Jovane, L., Yokoyama, E., Seda, T., Burmester, R. F., Trindade, R. I. F., & Housen, B. A. (2011). Rock magnetism of hematitic "bombs" from the Araguainha impact structure, Brazil. *Geochemistry, Geophysics, Geosystems*, *12*(12), Q12Z34. https://doi.org/10.1029/2011GC003758

Karlin, R. (1990). Magnetic mineral diagenesis in suboxic sediments at Bettis site W-N, NE Pacific ocean. *Journal of Geophysical Research*, *95*(B4), 4421–4436. https://doi.org/10.1029/JB095iB04p04421

Kawamura, N., Ishikawa, N., & Torii, M. (2012). Diagenetic alteration of magnetic minerals in Labrador Sea sediments (IODP Sites U1305, U1306, and U1307). *Geochemistry, Geophysics, Geosystems*, *13*(8), Q08013. https://doi.org/10.1029/2012GC004213

Kawamura, N., Oda, H., Ikehara, K., Yamazaki, T., Shioi, K., Taga, S., et al. (2007). Diagenetic effect on magnetic properties of marine core sediments from the southern Okhotsk Sea. *Earth, Planets and Space*, *59*(2), 83–93. https://doi.org/10.1186/BF03352680

King, J. G., Williams, W., Wilkinson, C. D. W., McVitie, S., & Chapman, J. N. (1996). Magnetic properties of magnetite arrays produced by the method of electron beam lithography. *Geophysical Research Letters*, *23*(20), 2847–2850. https://doi.org/10.1029/96GL01371

Kletetschka, G., & Wasilewski, P. J. (2002). Grain size limit for SD hematite. *Physics of the Earth and Planetary Interiors*, *129*(1-2), 173–179. https://doi.org/10.1016/S0031-9201(01)00271-0

Knowles, J. E. (1981). The properties of acicular particles of $(\gamma\text{-}Fe_2O_3)_x(Fe_3O_4)_{1-x}$. *Journal of Magnetism and Magnetic Materials*, *22*(3), 263–266. https://doi.org/10.1016/0304-8853(81)90031-7

Kopp, R. E., & Kirschvink, J. L. (2008). The identification and biogeochemical interpretation of fossil magnetotactic bacteria. *Earth Science Reviews*, *86*(1-4), 42–61. https://doi.org/10.1016/j.earscirev.2007.08.001

Krása, D., Wilkinson, C. D. W., Gadegaard, N., Kong, X., Zhou, H., Roberts, A. P., et al. (2009). Nanofabrication of two-dimensional arrays of magnetite particles for fundamental rock magnetic studies. *Journal of Geophysical Research*, *114*, B02104. https://doi.org/10.1029/2008JB006017

Kumari, M., Hirt, A. M., Uebe, R., Schüler, D., Tompa, É., Pósfai, M., et al. (2015). Experimental mixtures of superparamagnetic and single-domain magnetite with respect to Day-Dunlop plots. *Geochemistry, Geophysics, Geosystems*, *16*, 1739–1752. https://doi.org/10.1002/2015GC005744

Lanci, L. (2010). Detection of multi-axial magnetite by remanence effect on anisotropy of magnetic susceptibility. *Geophysical Journal International*, *181*, 1362–1366. https://doi.org/10.1111/j.1365-246X.2010.04588.x

Lanci, L., & Kent, D. V. (2003). Introduction of thermal activation in forward modeling of hysteresis loops for single-domain magnetic particles and implications for the interpretation of the Day diagram. *Journal of Geophysical Research*, *108*(B3), 2142. https://doi.org/10.1029/2001JB000944

Larrasoaña, J. C., Roberts, A. P., Chang, L., Schellenberg, S. A., Fitz Gerald, J. D., Norris, R. D., & Zachos, J. C. (2012). Magnetotactic bacterial response to Antarctic dust supply during the Palaeocene-Eocene thermal maximum. *Earth and Planetary Science Letters*, *333–334*, 122–133.

Larrasoaña, J. C., Roberts, A. P., Musgrave, R. J., Gràcia, E., Piñero, E., Vega, M., & Martínez-Ruiz, F. (2007). Diagenetic formation of greigite and pyrrhotite in gas hydrate marine sedimentary systems. *Earth and Planetary Science Letters*, *261*(3-4), 350–366. https://doi.org/10.1016/j.epsl.2007.06.032

Lascu, I., Harrison, R. J., Li, Y. T., Muraszko, J. R., Channell, J. E. T., Piotrowski, A. M., & Hodell, D. A. (2015). Magnetic unmixing of first-order reversal curve diagrams using principal component analysis. *Geochemistry, Geophysics, Geosystems*, *16*(9), 2900–2915. https://doi.org/10.1002/2015GC005909

Liu, J., Zhu, R. X., Roberts, A. P., Li, S. Q., & Chang, J. H. (2004). High-resolution analysis of early diagenetic effects on magnetic minerals in post-middle-Holocene continental shelf sediments from the Korea Strait. *Journal of Geophysical Research*, *109*, B03103. https://doi.org/10.1029/2003JB002813

Liu, Q. S., Deng, C. L., Torrent, J., & Zhu, R. X. (2007). Review of recent developments in mineral magnetism of the Chinese loess. *Quaternary Science Reviews*, *26*(3-4), 368–385. https://doi.org/10.1016/j.quascirev.2006.08.004

Maher, B. A. (1988). Magnetic properties of some synthetic sub-micron magnetites. *Geophysical Journal*, *94*(1), 83–96. https://doi.org/10.1111/j.1365-246X.1988.tb03429.x

Martín-Hernández, F., Dekkers, M. J., Bominaar-Silkens, I. M. A., & Maan, J. C. (2008). Magnetic anisotropy behaviour of pyrrhotite as determined by low- and high-field experiments. *Geophysical Journal International*, *174*(1), 42–54. https://doi.org/10.1111/j.1365-246X.2008.03793.x

McCabe, C., & Channell, J. E. T. (1994). Late Paleozoic remagnetization in limestones of the Craven Basin (northern England) and the rock magnetic fingerprint of remagnetized sedimentary carbonates. *Journal of Geophysical Research*, *99*(B3), 4603–4612. https://doi.org/10.1029/93JB02802

Ménabréaz, L., Thouveny, N., Camoin, G., & Lund, S. P. (2010). Paleomagnetic record of the late Pleistocene reef sequence of Tahiti (French Polynesia): A contribution to the chronology of the deposits. *Earth and Planetary Science Letters*, *294*(1-2), 58–68. https://doi.org/10.1016/j.epsl.2010.03.002

Mitra, R., Tauxe, L., & Gee, J. S. (2011). Detecting uniaxial single domain grains with a modified IRM technique. *Geophysical Journal International*, *187*(3), 1250–1258. https://doi.org/10.1111/j.1365-246X.2011.05224.x

Mitra, R., Tauxe, L., & Gee, J. S. (2012). Reply to comment by K. Fabian on 'Detecting uniaxial single domain grains with a modified IRM technique'. *Geophysical Journal International*, *191*(1), 46–50. https://doi.org/10.1111/j.1365-246X.2012.05605.x

Moores, E. M., & Twiss, R. J. (1995). *Tectonics* (p. 415). Long Grove, IL: Waveland Press.
Moskowitz, B. M. (1980). Theoretical grain size limits for single-domain, pseudo-single-domain and multi-domain behavior in titanomagnetite ($x = 0.6$) as a function of low-temperature oxidation. *Earth and Planetary Science Letters*, *47*(2), 285–293. https://doi.org/10.1016/0012-821X(80)90045-X
Muxworthy, A. R. (2013). The role of magnetic interactions in natural systems. *Astronomy and Geophysics*, *54*(2), 2.31–2.35. https://doi.org/10.1093/astrogeo/att036
Muxworthy, A. R., Heslop, D., & Williams, W. (2004). Influence of magnetostatic interactions on first-order-reversal-curve (FORC) diagrams: A micromagnetic approach. *Geophysical Journal International*, *158*(3), 888–897. https://doi.org/10.1111/j.1365-246X.2004.02358.x
Muxworthy, A. R., King, J. G., & Heslop, D. (2005). Assessing the ability of first-order reversal curve (FORC) diagrams to unravel complex magnetic signals. *Journal of Geophysical Research*, *110*, B01105. https://doi.org/10.1029/2004JB003195
Muxworthy, A. R., & Williams, W. (2005). Magnetostatic interaction fields in first-order-reversal curve diagrams. *Journal of Applied Physics*, *97*(6), 063905. https://doi.org/10.1063/1.1861518
Muxworthy, A. R., & Williams, W. (2009). Critical superparamagnetic/single domain grain sizes in interacting magnetite particles: Implications for magnetosome crystals. *Journal of the Royal Society Interface*, *6*(41), 1207–1212. https://doi.org/10.1098/rsif.2008.0462
Muxworthy, A. R., & Williams, W. (2015). Critical single-domain grain sizes in elongated iron particles: Implications for meteoritic and lunar magnetism. *Geophysical Journal International*, *202*(1), 578–583. https://doi.org/10.1093/gji/ggv180
Muxworthy, A. R., Williams, W., Roberts, A. P., Winklhofer, M., Chang, L., & Pósfai, M. (2013). Critical single domain grain sizes in chains of interacting greigite particles: Implications for magnetosome crystals. *Geochemistry, Geophysics, Geosystems*, *14*(12), 5430–5441. https://doi.org/10.1002/2013GC004973
Muxworthy, A. R., Williams, W., & Virdee, D. (2003). Effect of magnetostatic interactions on the hysteresis parameters of single-domain and pseudo-single-domain grains. *Journal of Geophysical Research*, *108*(B11), 2517. https://doi.org/10.1029/2003JB002588
Nagata, T. (1961). *Rock magnetism* (p. 366). Tokyo: Maruzen.
Nagata, T., & Carleton, B. J. (1987). Magnetic remanence coercivity of rocks. *Journal of Geomagnetism and Geoelectricity*, *39*(8), 447–461. https://doi.org/10.5636/jgg.39.447
Nagy, L., Williams, W., Muxworthy, A. R., Fabian, K., Almeida, T. P., Conbhuí, P. Ó., & Shcherbakov, V. P. (2017). Stability of equidimensional pseudo-single-domain magnetite over billion-year timescales. *Proceedings of the National Academy of Sciences of the United States of America*, *114*(10), 10,356–10,360. https://doi.org/10.1073/pnas.1708344114
Néel, L. (1949). Théorie du trainage magnétique des ferromagnétiques en grains fin avec application aux terres cuites. *Annals of Geophysics*, *5*, 99–136.
Néel, L. (1955). Some theoretical aspects of rock-magnetism. *Advances in Physics*, *4*(14), 191–243. https://doi.org/10.1080/00018735500101204
Nowaczyk, N. R. (2011). Dissolution of titanomagnetite and sulphidization in sediments from Lake Kinneret, Israel. *Geophysical Journal International*, *187*(1), 34–44. https://doi.org/10.1111/j.1365-246X.2011.05120.x
Ouyang, T., Heslop, D., Roberts, A. P., Tian, C., Zhu, Z., Qiu, Y., & Peng, X. (2014). Variable remanence acquisition efficiency in sediments containing biogenic and detrital magnetites: Implications for relative paleointensity signal recording. *Geochemistry, Geophysics, Geosystems*, *15*(7), 2780–2796. https://doi.org/10.1002/2014GC005301
Özdemir, Ö., & Dunlop, D. J. (1997). Effect of crystal defects and internal stress on the domain structure and magnetic properties of magnetite. *Journal of Geophysical Research*, *102*(B9), 20,211–20,224. https://doi.org/10.1029/97JB01779
Özdemir, Ö., & Dunlop, D. J. (2010). Hallmarks of maghemitization in low-temperature remanence cycling of partially oxidized magnetite nanoparticles. *Journal of Geophysical Research*, *115*, B02101. https://doi.org/10.1029/2009JB006756
Özdemir, Ö., & Dunlop, D. J. (2014). Hysteresis and coercivity of hematite. *Journal of Geophysical Research: Solid Earth*, *119*, 2582–2594. https://doi.org/10.1002/2013JB010739
Parry, L. G. (1982). Magnetization of immobilized particle dispersions with two distinct particle sizes. *Physics of the Earth and Planetary Interiors*, *28*(3), 230–241. https://doi.org/10.1016/0031-9201(82)90004-8
Passier, H. F., & Dekkers, M. J. (2002). Iron oxide formation in the active oxidation front above sapropel S1 in the eastern Mediterranean Sea as derived from low-temperature magnetism. *Geophysical Journal International*, *150*(1), 230–240. https://doi.org/10.1046/j.1365-246X.2002.01704.x
Paterson, G., Muxworthy, A. R., Roberts, A. P., & MacNiocaill, C. (2010). Assessment of the usefulness of lithic clasts from pyroclastic deposits for paleointensity determination. *Journal of Geophysical Research*, *115*, B03104. https://doi.org/10.1029/2009JB006475
Petersen, N., & Vali, H. (1987). Observation of shrinkage cracks in ocean floor titanomagnetites. *Physics of the Earth and Planetary Interiors*, *46*(1-3), 197–205. https://doi.org/10.1016/0031-9201(87)90182-8
Pike, C. R., Roberts, A. P., & Verosub, K. L. (1999). Characterizing interactions in fine magnetic particle systems using first order reversal curves. *Journal of Applied Physics*, *85*(9), 6660–6667. https://doi.org/10.1063/1.370176
Pósfai, M., Cziner, K., Márton, E., Márton, P., Buseck, P. R., Frankel, R. B., & Bazylinski, D. A. (2001). Crystal-size distributions and possible biogenic origin of Fe sulfides. *European Journal of Mineralogy*, *13*(4), 691–703. https://doi.org/10.1127/0935-1221/2001/0013-0691
Roberts, A. P. (1995). Magnetic characteristics of sedimentary greigite (Fe_3S_4). *Earth and Planetary Science Letters*, *134*(3-4), 227–236. https://doi.org/10.1016/0012-821X(95)00131-U
Roberts, A. P., Almeida, T. P., Church, N. S., Harrison, R. J., Heslop, D., Li, Y. L., et al. (2017). Resolving the origin of pseudo-single domain magnetic behavior. *Journal of Geophysical Research: Solid Earth*, *122*, 9534–9558. https://doi.org/10.1002/2017JB014860
Roberts, A. P., Chang, L., Heslop, D., Florindo, F., & Larrasoaña, J. C. (2012). Searching for single domain magnetite in the 'pseudo-single-domain' sedimentary haystack: Implications of biogenic magnetite preservation for sediment magnetism and relative paleointensity determinations. *Journal of Geophysical Research*, *117*, B08104. https://doi.org/10.1029/2012JB009412
Roberts, A. P., Chang, L., Rowan, C. J., Horng, C.-S., & Florindo, F. (2011). Magnetic characteristics of sedimentary greigite (Fe_3S_4): An update. *Reviews of Geophysics*, *49*, RG1002. https://doi.org/10.1029/2010RG000336
Roberts, A. P., Cui, Y. L., & Verosub, K. L. (1995). Wasp-waisted hysteresis loops: Mineral magnetic characteristics and discrimination of components in mixed magnetic systems. *Journal of Geophysical Research*, *100*(B9), 17,909–17,924. https://doi.org/10.1029/95JB00672
Roberts, A. P., Florindo, F., Chang, L., Heslop, D., Jovane, L., & Larrasoaña, J. C. (2013). Magnetic properties of pelagic marine carbonates. *Earth Science Reviews*, *127*, 111–139. https://doi.org/10.1016/j.earscirev.2013.09.009
Roberts, A. P., Florindo, F., Larrasoaña, J. C., O'Regan, M. A., & Zhao, X. (2010). Complex polarity pattern at the former Plio-Pleistocene global stratotype section at Vrica (Italy): Remagnetization by magnetic iron sulphides. *Earth and Planetary Science Letters*, *292*(1-2), 98–111. https://doi.org/10.1016/j.epsl.2010.01.025
Roberts, A. P., Heslop, D., Zhao, X., & Pike, C. R. (2014). Understanding fine magnetic particle systems through use of first-order reversal curve diagrams. *Reviews of Geophysics*, *52*(4), 557–602. https://doi.org/10.1002/2014RG000462

Roberts, A. P., Jiang, W. T., Florindo, F., Horng, C. S., & Laj, C. (2005). Assessing the timing of greigite formation and the reliability of the Upper Olduvai polarity transition record from the Crostolo River, Italy. *Geophysical Research Letters*, *32*, L05307. https://doi.org/10.1029/2004GL022137

Roberts, A. P., Pike, C. R., & Verosub, K. L. (2000). First-order reversal curve diagrams: A new tool for characterizing the magnetic properties of natural samples. *Journal of Geophysical Research*, *105*(B12), 28,461–28,475. https://doi.org/10.1029/2000JB900326

Roberts, A. P., Reynolds, R. L., Verosub, K. L., & Adam, D. P. (1996). Environmental magnetic implications of greigite (Fe_3S_4) formation in a 3 my lake sediment record from Butte Valley, northern California. *Geophysical Research Letters*, *23*(20), 2859–2862. https://doi.org/10.1029/96GL02831

Roberts, A. P., Sagnotti, L., Florindo, F., Bohaty, S. M., Verosub, K. L., Wilson, G. S., & Zachos, J. C. (2013). Environmental magnetic record of paleoclimate, unroofing of the Transantarctic Mountains, and volcanism in late Eocene to early Miocene glaci-marine sediments from the Victoria Land Basin, Ross Sea, Antarctica. *Journal of Geophysical Research: Solid Earth*, *118*, 1845–1861. https://doi.org/10.1002/jgrb.50151

Roberts, A. P., Verosub, K. L., Weeks, R. J., Lehman, B., & Laj, C. (1995). Mineral magnetic properties of Middle and Late Pleistocene sediments at ODP sites 883, 884, and 887, North Pacific Ocean. *Proceedings. Ocean Drilling Program. Scientific Results*, *145*, 483–490.

Rochette, P., Fillion, G., Mattéi, J.-L., & Dekkers, M. J. (1990). Magnetic transition at 30-34 Kelvin in pyrrhotite: Insight into a widespread occurrence of this mineral in rocks. *Earth and Planetary Science Letters*, *98*(3-4), 319–328. https://doi.org/10.1016/0012-821X(90)90034-U

Rowan, C. J., Roberts, A. P., & Broadbent, T. (2009). Reductive diagenesis, magnetite dissolution, greigite growth and paleomagnetic smoothing in marine sediments: A new view. *Earth and Planetary Science Letters*, *277*(1-2), 223–235. https://doi.org/10.1016/j.epsl.2008.10.016

Schabes, M. E., & Bertram, H. N. (1988). Magnetization processes in ferromagnetic cubes. *Journal of Applied Physics*, *64*(3), 1347–1357. https://doi.org/10.1063/1.341858

Smirnov, A. V. (2007). Effect of the magnetic field applied during cooling on magnetic hysteresis in the low-temperature phase of magnetite: First-order reversal curve (FORC) analysis. *Geochemistry, Geophysics, Geosystems*, *8*(8), Q08005. https://doi.org/10.1029/2007GC001650

Smirnov, A. V., & Tarduno, J. A. (2000). Low-temperature magnetic properties of pelagic sediments (Ocean Drilling Program Site 805C): Tracers of maghemitization and magnetic mineral reduction. *Journal of Geophysical Research*, *105*(B7), 16,457–16,471. https://doi.org/10.1029/2000JB900140

Smith, B. M. (1987). Consequences of the maghemitization on the magnetic properties of submarine basalts: Synthesis of previous works and results concerning basement rocks from mainly D.S.D.P. Legs 51 and 52. *Physics of the Earth and Planetary Interiors*, *46*(1-3), 206–226. https://doi.org/10.1016/0031-9201(87)90183-X

Soffel, H. C. (1977). Pseudo single domain effects and single domain—Multidomain transition in natural pyrrhotite deduced from domain structure observations. *Journal of Geophysics*, *42*, 351–359.

Soffel, H. C., & Appel, E. (1982). Domain structure of small synthetic titanomagnetite particles and experiments with IRM and TRM. *Physics of the Earth and Planetary Interiors*, *30*(4), 348–355. https://doi.org/10.1016/0031-9201(82)90042-5

Sprowl, D. R. (1990). Numerical estimation of interactive effects in single-domain magnetite. *Geophysical Research Letters*, *17*(11), 2009–2012. https://doi.org/10.1029/GL017i011p02009

Stacey, F. D. (1961). Theory of the magnetic properties of igneous rocks in alternating fields. *Philosophical Magazine*, *6*(70), 1241–1260. https://doi.org/10.1080/14786436108243374

Stoner, E. C., & Wohlfarth, E. P. (1948). A mechanism of magnetic hysteresis in heterogeneous alloys. *Philosophical Transactions of the Royal Society of London*, *A240*, 599–642.

Swanson-Hysell, N. L., Maloof, A. C., Kirschvink, J. L., Halverson, G. P., & Hurtgen, M. T. (2012). Constraints on Neoproterozoic paleogeography and Paleozoic orogenesis from paleomagnetic records of the Bitter Springs Formation, Amadeus Basin, central Australia. *American Journal of Science*, *312*(8), 817–884. https://doi.org/10.2475/08.2012.01

Tarduno, J. A. (1994). Temporal trends of magnetic dissolution in the pelagic realm: Gauging paleoproductivity? *Earth and Planetary Science Letters*, *123*(1-3), 39–48. https://doi.org/10.1016/0012-821X(94)90255-0

Tarduno, J. A. (1995). Superparamagnetism and reduction diagenesis in pelagic sediments—Enhancement or depletion? *Geophysical Research Letters*, *22*(11), 1337–1340. https://doi.org/10.1029/95GL00888

Tarduno, J. A., & Myers, M. (1994). A primary magnetization fingerprint from the Cretaceous Laytonville Limestone: Further evidence for rapid oceanic plate velocities. *Journal of Geophysical Research*, *99*(B11), 21,691–21,703. https://doi.org/10.1029/94JB01939

Tarduno, J. A., Tian, W. L., & Wilkison, S. (1998). Biogeochemical remanent magnetization in pelagic sediments of the western equatorial Pacific Ocean. *Geophysical Research Letters*, *25*(21), 3987–3990. https://doi.org/10.1029/1998GL900079

Tarduno, J. A., & Wilkison, S. (1996). Non-steady state magnetic mineral reduction, chemical lock-in, and delayed remanence acquisition in pelagic sediments. *Earth and Planetary Science Letters*, *144*(3-4), 315–326. https://doi.org/10.1016/S0012-821X(96)00174-4

Tauxe, L., Bertram, H. N., & Seberino, C. (2002). Physical interpretation of hysteresis loops: Micromagnetic modeling of fine particle magnetite, *Geochemistry, Geophysics, Geosystems*, *3*, 1055. https://doi.org/10.1029/2001GC000241

Tauxe, L., Butler, R., Banerjee, S. K., & van der Voo, R. (2010). *Essentials of paleomagnetism*. Berkeley, CA: University of California Press. Available online at: https://earthref.org/MagIC/books/Tauxe/Essentials/.

Tauxe, L., Mullender, T. A. T., & Pick, T. (1996). Potbellies, wasp-waists, and superparamagnetism in magnetic hysteresis. *Journal of Geophysical Research*, *101*(B1), 571–583. https://doi.org/10.1029/95JB03041

Thornhill, R. H., Burgess, J. G., Sakaguchi, T., & Matsunaga, T. (1994). A morphological classification of bacteria containing bullet-shaped magnetic particles. *FEMS Microbiology Letters*, *115*(2-3), 169–176. https://doi.org/10.1111/j.1574-6968.1994.tb06633.x

Till, J. L., Jackson, M. J., Rosenbaum, J. G., & Solheid, P. (2011). Magnetic properties in an ash flow tuff with continuous grain size variation: A natural reference for magnetic particle granulometry. *Geochemistry, Geophysics, Geosystems*, *12*(7), Q07Z26. https://doi.org/10.1029/2011GC003648

Torii, M. (1997). Low-temperature oxidation and subsequent downcore dissolution of magnetite in deep-sea sediments, ODP Leg 161 (western Mediterranean). *Journal of Geomagnetism and Geoelectricity*, *49*(10), 1233–1245. https://doi.org/10.5636/jgg.49.1233

Valet, J.-P., Meynadier, L., & Guyodo, Y. (2005). Geomagnetic dipole strength and reversal rate over the past two million years. *Nature*, *435*(7043), 802–805. https://doi.org/10.1038/nature03674

van Velzen, A. J., & Zijderveld, J. D. A. (1995). Effects of weathering on single-domain magnetite in Early Pliocene marine marls. *Geophysical Journal International*, *121*(1), 267–278. https://doi.org/10.1111/j.1365-246X.1995.tb03526.x

von Dobeneck, T. (1996). A systematic analysis of natural magnetic mineral assemblages based on modelling hysteresis loops with coercivity-related hyperbolic basis functions. *Geophysical Journal International*, *124*(3), 675–694. https://doi.org/10.1111/j.1365-246X.1996.tb05632.x

Weaver, R., Roberts, A. P., & Barker, A. J. (2002). A late diagenetic (syn-folding) magnetization carried by pyrrhotite: Implications for paleomagnetic studies from magnetic iron sulphide-bearing sediments. *Earth and Planetary Science Letters*, *200*(3-4), 371–386. https://doi.org/10.1016/S0012-821X(02)00652-0

Wehland, F., Stancu, A., Rochette, P., Dekkers, M. J., & Appel, E. (2005). Experimental evaluation of magnetic interaction in pyrrhotite bearing samples. *Physics of the Earth and Planetary Interiors*, *153*(4), 181–190. https://doi.org/10.1016/j.pepi.2005.05.006

Wohlfarth, E. P. (1958). Relations between different modes of acquisition of the remanent magnetization of ferromagnetic particles. *Journal of Applied Physics*, *29*(3), 595–596. https://doi.org/10.1063/1.1723232

Wasilewski, P. J. (1973). Magnetic hysteresis in natural materials, *Earth and Planetary Science Letters*, *20*(1), 67–72. https://doi.org/10.1016/0012-821X(73)90140-4.

Xu, W., van der Voo, R., & Peacor, D. R. (1998). Electron microscopic and rock magnetic study of remagnetized Leadville carbonates, central Colorado. *Tectonophysics*, *296*(3-4), 333–362. https://doi.org/10.1016/S0040-1951(98)00146-2

Yamazaki, T., Abdeldayem, A. L., & Ikehara, K. (2003). Rock-magnetic changes with reduction diagenesis in Japan Sea sediments and preservation of geomagnetic secular variation in inclination during the last 30,000 years. *Earth, Planets and Space*, *55*(6), 327–340. https://doi.org/10.1186/BF03351766

Yamazaki, T., & Ioka, N. (1997). Environmental rock-magnetism of pelagic clay: Implications for Asian eolian input to the North Pacific since the Pliocene. *Paleoceanography*, *12*(1), 111–124. https://doi.org/10.1029/96PA02757

Zhao, X., Roberts, A. P., Heslop, D., Paterson, G. A., Li, Y. L., & Li, J. H. (2017). Magnetic domain state diagnosis using hysteresis reversal curves. *Journal of Geophysical Research: Solid Earth*, *122*, 4767–4789. https://doi.org/10.1002/2016JB013683

Ziegler, L. B., Constable, C. G., Johnson, C. L., & Tauxe, L. (2011). PADM2M: A penalized maximum likelihood model of the 0–2 Ma palaeomagnetic axial dipole moment. *Geophysical Journal International*, *184*(3), 1069–1089. https://doi.org/10.1111/j.1365-246X.2010.04905.x